

MIXING OVER SHALLOW CORAL REEFS IN RELATION TO THE REEF RUGOSITY

Msc Thesis Jente van Leeuwe



Wageningen University, INREEF & WMR

Supervisors WUR: Bart Vermeulen & Roxanne Fransisca-Liana
supervisor WMR: Droguer Gulsah

Abstract

Increasing inflows of nutrients to shallow coral reefs are an important stressor in ongoing global reef degradation. Previous research has indicated that there are often major nutrient flows from terrestrial sources to the degrading coral reefs. To better understand the importance of nutrient flow to the coral reefs, a clearer understanding of the coastal hydrodynamics and mixing processes transporting these nutrients, is necessary. This research has aimed to assess the role of reef rugosity on the mixing processes in shallow coral reefs. Two 25h ADCP measurements were performed on four different sites on the west coast of Bonaire, together with various rugosity measurements on each site. The sites were chosen based on an assumed differences in rugosity. Friction factors were calculated to assess the influence of rugosity on the turbulence and mixing in the water column. The collected data showed the currents to be wind dominated, with low average velocities of 0-0.1 m/s. The currents did not seem affected by the rugosity, with changes in current velocity similarly correlated to changes in wind forcing for both high and low rugosity areas. Higher rugosity did seem to give higher friction factors, although only weak correlations were found due to the low flow velocities. The results suggested that during high flow velocity periods more nutrients could be trapped in the coral reefs, due to increased turbulence around the reef surfaces. This could be even more relevant considering the fact that high flow velocities often occur during rain and storm events, which are important nutrients inputs through freshwater discharge. However, due to high uncertainties in the friction factor calculations, these relations cannot be taken as scientific proof but rather as indications for further research.

Content

1.INTRODUCTION	1
1.1 RESEARCH OBJECTIVES	2
1.2 RESEARCH QUESTIONS	3
2.SITE DESCRIPTION	3
2.1 CLIMATE	3
2.2 CURRENTS AND COAST	3
3.METHODS	5
3.1 DATA GENERATION	5
3.2 MEAN CURRENTS (RQ 1)	6
3.3 RUGOSITY (RQ 2)	7
3.4 FRICTION FACTOR (RQ 3).....	8
4.RESULTS	9
4.1 MEAN CURRENTS (RQ1)	9
4.2 RUGOSITY (RQ2)	11
4.3 FRICTION FACTOR (RQ3)	12
5.DISCUSSION	14
5.1 CURRENTS (RQ 1 & 3)	14
5.2 RUGOSITY AND FRICTION FACTOR (RQ 2 & 3)	15
6.CONCLUSION	17
6.1 ACKNOWLEDGEMENTS	17
7.REFERENCES	18
8.APPENDICES	21

1.Introduction

Coral reefs are a vital cog in the coastal water ecosystems all over the world. They are a sustaining factor in the food chain and provide enormous amounts of species with food sources, shelter from predators and a location for egg hatching (Vanwonderghem & Webster, 2020). Apart from this important role in the ecosystem they also provide us with opportunities for fishing and leisure and serve as an important shore protection mechanism with their ability to work as shock breakers for the coast (Woodhead et al., 2019). Nowadays, these coral reefs are threatened all over the world by climate change and local stressors, like sea temperature rise, pollution and overfishing (Morais et al., 2020; Sandin et al., 2008). This has resulted worldwide in a drastic decline in coral cover and coral-related species diversity (de Bakker et al., 2016; Stokes et al., 2010).

A key factor for the health of coral reefs is nutrient supply. Coral reefs generally thrive in low nutrient environments and studies have confirmed that an overload of nutrients in coral reef areas makes them more vulnerable to degradation (DeCarlo et al., 2020; Edmunds & Burgess, 2018; Stocking et al., 2018). Increased nutrient supply can create an environment that favours the species that drive coral bleaching. Thus, when the water temperature increases, bleaching events will be more severe under high nutrient conditions (DeCarlo et al., 2020). Therefore, it is essential to know how nutrients are transported over coral reef areas. For example, low transport might result in a long residence time of nutrients in the reefs, and thus a stronger effect on the reefs. On the other hand, low transport can result in little vertical mixing, so less nutrients might be introduced into the reef (Burchard et al., 2008). To study the transport of nutrients in coral reef areas, it is good to start with the general water transport over reef areas, as the transport of mass and nutrients are closely related (DeCarlo et al., 2020).

Over large distances, this transport is determined by the ocean currents around a coral reef island.

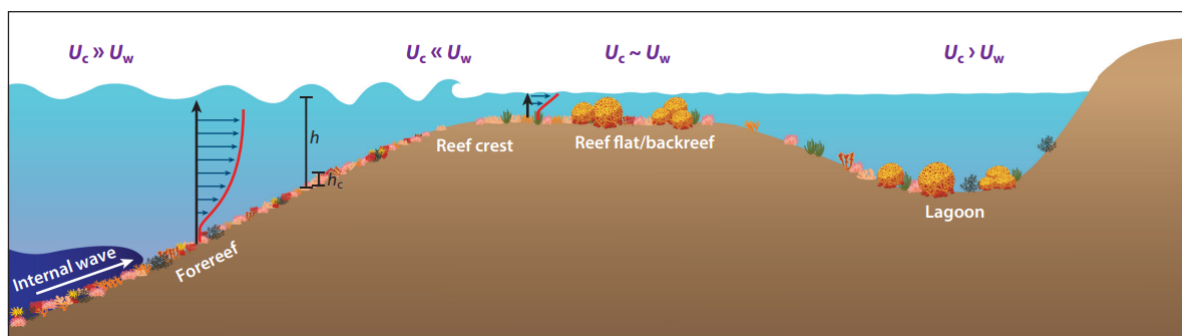


Figure 1: Overview of the different hydrological zones in coral reef areas, with U_c the mesoscale current and U_w the wave driven current (Davis et al., 2021).

On a reef wide scale, the horizontal transport is governed by the main ocean currents, current deflection by the topography, buoyancy, and tidal motions (Figure 1, left part, where the mesoscale current (U_c) \gg the wave driven current (U_w)) (Davis et al., 2021; Hoitink, 2003; Monismith, 2007). Wolanski et al. (1984) proposed a model that showed how the general flow direction, forced by the trade winds, evolved around small tropical islands. The model proposes that the incoming current is bend around the island. In the wake of the island, these currents turn inward, resulting into two counter rotating eddies in the leeside of the island. Hoitink (2003) added that these counter rotating eddies can create an Ekman benthic boundary layer, which results in a net downwelling near the coast.

Close to the coast, where the sea is shallower, other processes get involved. Here, the large scale currents are influenced by the reef rugosity creating bottom shear stress and surface wave processes are at play (Figure 1, middle part, where $U_c \ll U_w$ & $U_c \sim U_w$) (Davis et al., 2021). At the surface, incoming surface waves generate a net transport in the direction of the wave propagation, the Stokes drift (Bremer & Breivik, 2018). Due to bottom shear stress the waves will start to shoal, which will result in wave breaking. This breaking of the waves increases the transport in the wave direction. However, when the water is too shallow, the bottom shear stress is expected to be so large that the flow will decrease again (Monismith, 2007). Thus, an optimum in wave transport is expected where the wave shoaling balances the bottom shear stress (Hearn, 1999). Where this optimum will be is dependent on the reef rugosity. The wave induced flow also pushes up water to the coast, creating a pressure gradient that results in an offshore flow over the bottom, the undertow. The strength of this undertow is also largely dependent on the reef rugosity (Bremer & Breivik, 2018).

Furthermore, the reef is also an important driver in the vertical mixing over the water column. Increased bed shear stress, induced by high rugosity in coral reefs, creates vertical mixing through turbulent motions (Davis et al., 2021; Edmunds & Burgess, 2018; Hearn, 1999; Monismith, 2007; Stocking et al., 2018). However, the turbulence is also dependent on the flow velocity. A higher flow velocity will result in more turbulence (Davis et al., 2021). So, here as well, an optimum should be expected, but then in vertical mixing, where the bed shear stress creates turbulence, but does not decrease the flow velocity too much.

Multiple studies have already been performed on the role of reef rugosity on these processes. Teneva et al. (2013) observed high vertical fluxes under slow currents and related this to strong vertical mixing due to high reef rugosity. Rogers et al. (2018) investigated the relation between the terrain complexity and the bed roughness and found that for the bed roughness, moderate horizontal scales ($\sim 50\text{m}$) were dominant.

These secondary flow patterns discussed above and the nutrient transport that follows from it are of vital importance to the coral colonies. Previous studies have gained insight in the effect of reef roughness on separate processes. These studies report that higher reef rugosity leads to a higher shear resulting in a slowing down of the general current and thus of the horizontal transport (Bergquist & Boyle, 2006; Chase et al., 2005; Cole et al., 1985; Dunckley et al., 2012; Hearn, 1999). Also, in shallow areas, a higher reef rugosity has a strong effect on wave dissipation, creating increased turbulence (Hearn, 2011; Osorio-Cano et al., 2019). However, how these different processes affected by reef rugosity combine to create the vertical and horizontal transport is still unclear. Under the influence of reef rugosity, the balance between the different forcings on the current could be different. To gain a further understanding of the nutrient flows over a coral reef, it is necessary to gain a better understanding of the effect of reef rugosity on the net mixing over shallow reef areas (Davis et al., 2021; Teneva et al., 2013).

1.1 Research objectives

This project aims to give a better understanding on how the different transport processes over shallow reef areas are influenced by the rugosity of the reef, differing due to reef cover. In shallow reef areas the transport, both in vertical and horizontal direction are influenced by reef rugosity, which in turn is influenced by reef cover. A better understanding of these processes could help our knowledge on nutrient transport in shallow reef areas and ultimately lead to a better protection of shallow coral reefs.

1.2 Research questions

Main question: What is the influence of reef rugosity on the coastal transport and turbulent mixing over shallow coral reefs?

RQ1) What is the turbulent mixing over shallow reef areas and what are the governing processes of the coastal water transport?

RQ2) How does the reef rugosity change between different reef covers?

RQ3) How does the bed shear stress of the reef change between different reef covers?

2. Site description

2.1 Climate

Bonaire has a warm and dry climate with temperatures around the 30 °C and an average precipitation of ~460 mm/y (Hylkema et al., 2015). There is almost consistently an easterly wind over the island, due to its position in the trade winds. During the summer months, this can result in tropical storms on the island (Engel et al., 2012). Due to its position close to the equator and the resulting high temperatures, the sea temperature averages ~27 °C with minima and maxima of ~25 and ~28 °C (Frade et al., 2019).

2.2 Currents and coast

The easterly wind is also an important driver of the ocean currents around Bonaire. So, the general current around Bonaire is from east to west. The west side is therefore relatively calm, sheltered from the wind driven ocean currents coming from the east. The data for this research were collected on the west (lee) side of Bonaire, as on the east side the sea is considered too rough to perform

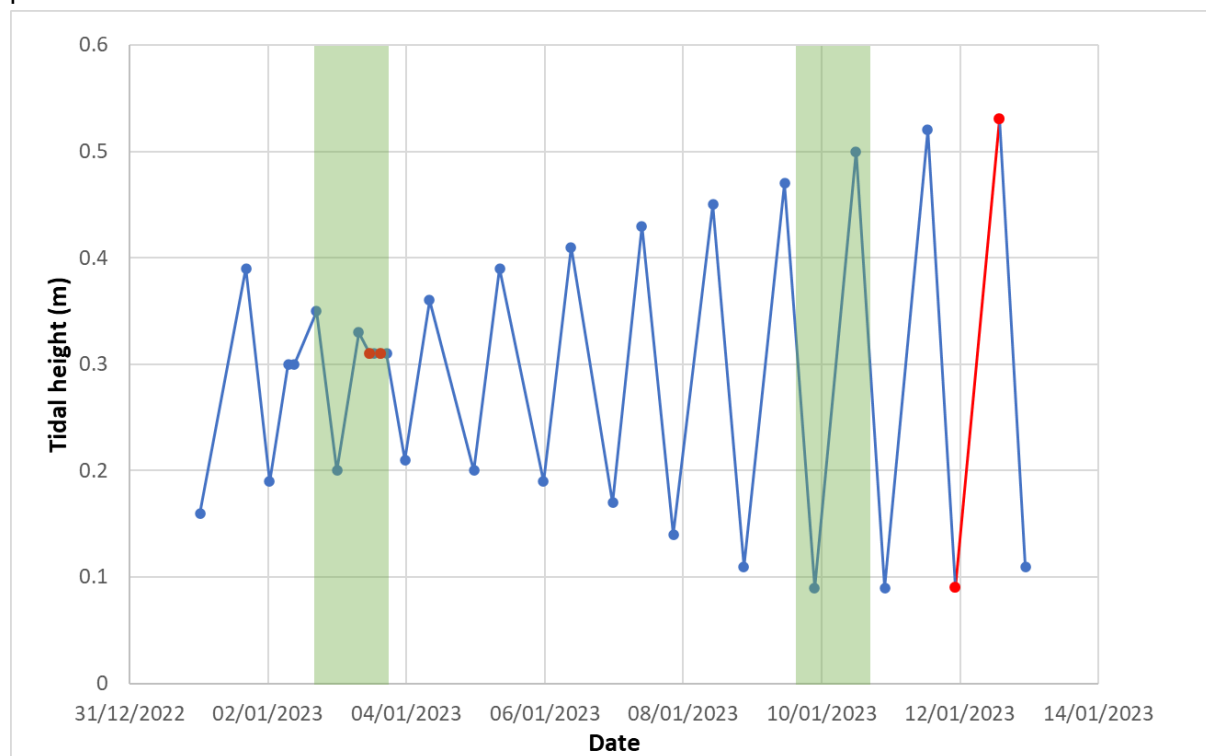


Figure 2: Example of the tides around the measurements at Bsc Beach (green), with the spring and neap tides marked in red (tides: Seatemperatu.re, 2023)

the measurements. On the west side, in the sheltered part of the island, wave energy is relatively low, with wave heights varying from 0-30 cm close to Kralendijk (the most sheltered part), to 1-1,5m at the north west point of the island (Engel et al., 2012; van Duyl, 1985). Also, the tidal amplitude is small, around 30 cm average along the west coast (Figure 2) (Hylkema et al., 2015). The west side of Bonaire has a diurnal amplitude, with a clear spring-neap cycle. The tidal amplitude at Kralendijk varies from close to zero during neap tide to ~40 cm during spring tide.

The water entry along the coast along the west coast is marked by a cliff coast from Kralendijk northward, with straight drops of at least 2m into the water, and more gentle coasts to the south, where there are beaches from sand and dead coral pieces. Once underwater, the bathymetry follows the same pattern all along the coast. Everywhere along the coast, shallow terrasses stretch out, descending steadily to a drop-off where the slope increases rapidly. This drop off is around 5-12m depth, extending to 30-40m depth, where another terrasse is found (Sandin et al., 2008). The shallow terrasses vary in width, from 50-250m, where the widest terrasses are found at the south of the west coast (Van Leeuwen, 2022).

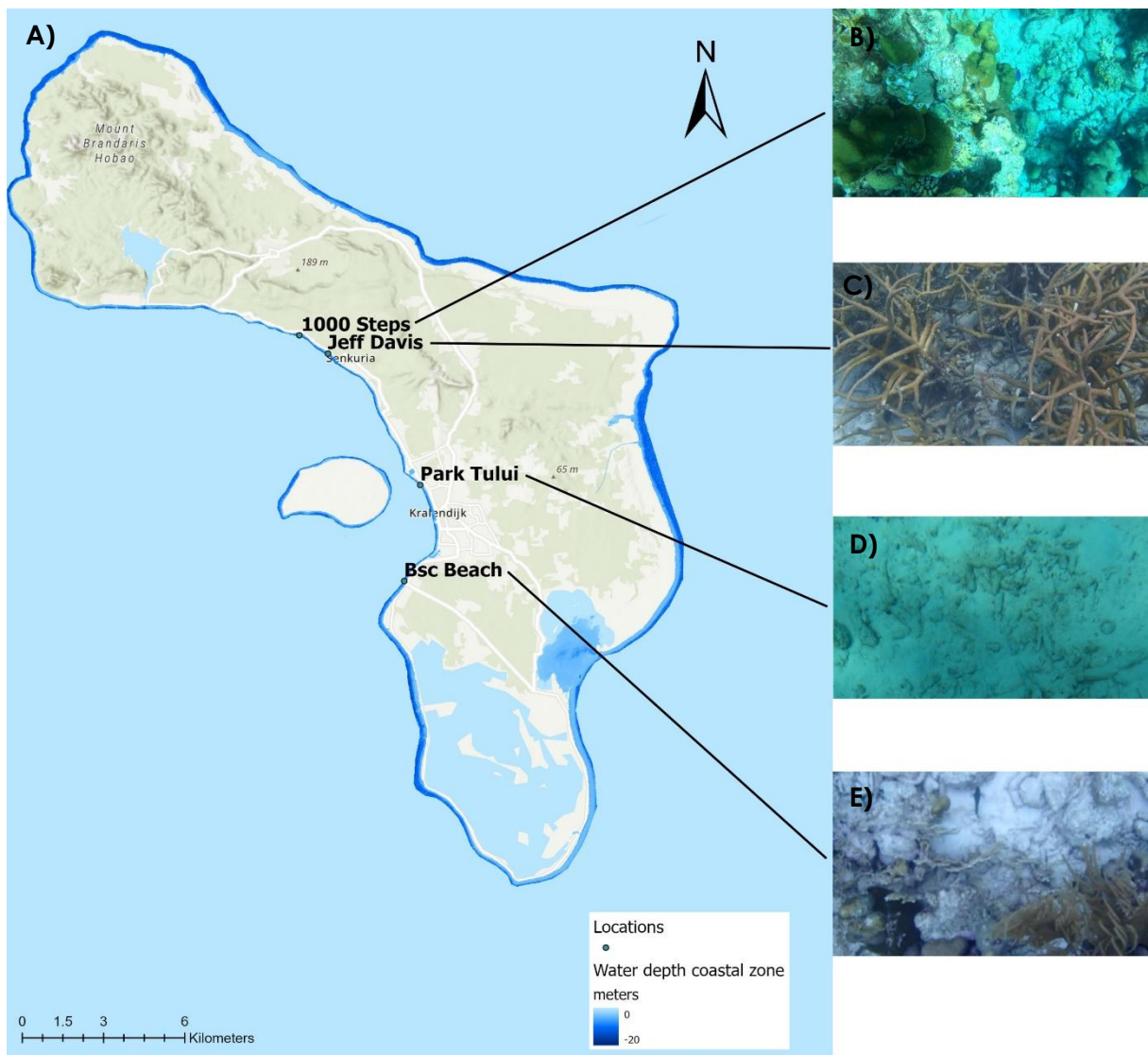


Figure 3: Map of Bonaire with the measurement locations (A) and pictures of the reef on each location (Esri, NASA, NGA, USGS, GIS4C, Grupo Ingeolan C.A., Kadaster Netherlands, Esri, HERE, Garmin, Foursquare, METI/NASA, USGS)

3.Methods

3.1 Data generation

The data collection took place during a field campaign from December 2022 until February 2023. During this period Acoustic Doppler Current Profiler (ADCP) and rugosity measurements were performed on four locations along the west coast of Bonaire. On the four locations, seven moored ADCP measurement of 24-26h and 2 transect measurements by boat were done. In addition to that, three different kinds of rugosity/ reef health assessments were performed on each location. The locations were chosen based on their expected differences in rugosity, which made them ideal for investigating the effects of the reef rugosity on the coastal currents and turbulent mixing in shallow reef areas. In Table 1 the date and locations for all measurements is shown, together with the depth and distance to the shore of the drop-off.

Table 1: General information of the ADCP measurements

Site	Coordinates (°N, °W)	Drop-off depth (m)	Distance coast-drop-off (m)	Current direction	Moored ADCP dates	Transect ADCP dates
Park Tului	12.159392, -68.282068	6	70	N	31-01-23 & 07-02-23	-
Bsc Beach	12.126785, -68.287578	9	80	N	02-01-23 & 09-01-23	09-01-23
Jeff Davis	12.204097, -68.313162	5	40	N	16-01-23 & 06-02-23	16-01-23
1000 Steps	12.210423, -68.322882	10	100	S	19-01-23 & -	-

Park Tului is located right in front Kralendijk where the distance between Bonaire and Klein Bonaire is smallest. The location is marked by a boulevard directly along the coast and docking places for sailing boats in the shallow area. Under water, the seafloor of the shallow terrasse is nearly flat with sand and dead coral pieces.

Bsc Beach lies in front of a neighbourhood south of Kralendijk. Despite that Bsc Beach lies in the south, the coast is a cliff into shallow water at this place. Near the coast the sea floor is sandy, but from 4m depth rubble from dead corals lying on the sand creates relief on the seafloor. Close to the drop-off some living corals are present as well.

Jeff Davis lies north of Kralendijk and is a site where reef restoration is done in the shallow areas. The site has a cliff coast into the sea. The sea floor on the shallow terrasse is mostly a combination of sand and dead coral pieces. However, close to the drop-off, around 4-5m deep there is a large thick patch of restored reef.

1000 Steps is the location with the most living corals on the shallow terrasse. From a cliff, there is a narrow beach at the coast. Under water, there are immediately patches of living corals to be found. The cover only increases with distance from the coast. The substantial amounts of hard corals create a strong relief on the sea floor.

3.2 Mean currents (RQ 1)

The moored ADCP measurements were performed with an 1200Hz workhorse ADCP connected to a battery case, which held two battery packs. Measurements of 24-26 consecutive hours were done twice on all four locations, with one week between the two measurements. Only at 1000 Steps one measurement was done, due to a malfunction with the connection to the battery case. A measurement time of 24-26 hours was chosen, so that a full tidal cycle would be completed during every session. Furthermore, the week between two measurements ensured that a comparison could be made between spring and neap tide. Ideally one measurement was performed during spring tide and one during neap tide. However, due to boat and diver availability restrictions this was not always possible.

For the measurements, a plan was developed in PlanADCP that allowed that all the measurements to be done without a battery shortage (see Appendix 8.1 for the PlanADCP commands). To be able to measure for 24 hours, without exhausting the battery, burst measurements were done. During a measurement, the ADCP would measure ensembles at 1.18 Hz for half an hour every hour. Every ensemble consisted of three sub-pings. The velocities were measured with 0.1 or 0.2m depth cell size. The first measurements were done with 0.1m depth cell size, but after a revision, this was changed to a 0.2m depth cell size. Once the measurement plan was communicated to the ADCP using BBtalk, the ADCP was attached to a 1.4x1.4m cross-frame and brought to the location, together with the battery, by two divers (see Figure 4 for the measurement set-up). This could be done either from shore or from a boat. When the ADCP was placed on the sea floor, on a sandy patch to not damage the corals, the ADCP would be placed a horizontal as possible, to minimize measurement errors.



Figure 4: Example of a moored ADCP measurement set-up

For the transect measurements, the methods of Van Leeuwen (2022) were followed. The transect measurements were done using the same ADCP but connected to a car battery placed in the boat instead. Due to problems with the connection of the ADCP and the battery, no transect measurements were done at Park Tului and 1000 Steps. During the measurements, the ADCP would be attached upside down to the ladder of the boat and fully submerged into the water. Transects were then measured from as close to the coast as the boat could go, to past the drop-off, to make sure the entire shallow terrace would be measured. Data were recorded up to 20 m depth. The transects were done 8 times per location with a boat speed below 1,5 m/s, to obtain enough data for analysis. A GPS device was used to record the location during the measurements. Because of a double sensor in the GPS, it did not only record the location, but also the shifts in boat direction. This way, correction for the boat movement could be done on the ADCP data. The ADCP and GPS were located close together (~0.5m), to get the best ADCP locations. Both the

ADCP data and the GPS data were combined immediately during the measurement using Winriver II. The obtained data could then be exported and further analysed.

Before analyses of the ADCP data could be performed, the data were cleaned up. First, the measured velocities were rotated to get a longshore (U), cross-shore (V) and vertical (W) velocity. With the positive direction always in the northern, offshore, and upward direction. The data sets were then cut so that it contained only measurements at the location and in the water column. Lastly, erroneous values were filtered out, caused by disturbances such as objects coming in the ADCP beam or lack of signal. This meant in practice, excluding all data with an error velocity lower than -0.3 m/s and higher than 0.3 m/s. For the analyses, the measurements were averaged per hour. This was done in order to obtain an impression of the currents and their temporal changes along the coast. To analyse tidal currents the hourly averaged data were depth averaged as well. This way, tidal currents were obtained as changes in direction or in strength of the currents over time. The resulting data could then be compared with tidal data from measurement stations on Bonaire to see if strong tidal currents are present.

3.3 Rugosity (RQ 2)

Transects

Rugosity transects were taken at all the sites. The transects consisted of four 10m transects at every location, two alongshore and two cross-shore. The transects were done around the location of the moored ADCP measurements. At each transect, the reef height was measured at a one-meter interval. The standard deviation of the height measurements was a measure of the rugosity at the location. The measurements were done diving, laying down a measuring tape and measuring the height at every meter using a measuring stick.

3D-model

At every location, a 10x10m square was filmed, to develop a 3D-model of the location. With this 3D-model it was possible to perform virtual rugosity chain measurement. For the filming of an area, a square was set out with reebars at the corner points. The square was made using a compass (for 90° angles) and measuring tape (for 10m distance). In the square reference objects were placed, so that distances could be determined in the 3D-model (see Appendix 8.1 for the reference objects and their size). The square was then filmed in a raster pattern, so that every part was covered twice. Also, the location of the corner reebars was obtained, to be able to locate the square later. The film thus obtained was later used to develop the 3D-model.






The 3D-model development was done using Free Video to JPG Converter and Metashape Agisoft. First images were extracted in Free Video to JPG Converter from the film at a 10-frame interval, to make sure that there was enough overlap between pictures to combine them (60-80%). These images were then loaded in Metashape Agisoft. There, the images would be aligned to create a point cloud. From this point cloud a mesh could be created, to which the texture could then be added to finish the model (see Figure 3). With Metashape Agisoft it was then also possible to measure in a straight line and following the coral reef. The ratio of these distances was used as an additional measure for reef rugosity.

HAS Score

Apart from the rugosity measurements a visual assessment of the reef health was done with the HAS score, following the method from Gratwicke & Speight (2005). This method distinguishes different areas based on various categories of reef health, instead of its geometry. Table 2 shows the various categories that are assessed with the HAS score. The HAS-score was done at every

site during a dive. All HAS-scores were done by one person, to avoid a bias. The scores from 1-5 were averaged over all categories to a HAS-score at all locations. The average of the scores from 1-5 gives an indication of the reef health/complexity.

Table 2: HAS-score rating system (Gratwicke & Speight, 2005)

	Score 1	2	3	4	5
Rugosity (Visual topographic estimate of the substratum in each quadrat)					
Variety of growth forms (Stalked/lobed/filamentous/ribbonlike/massive/branching/cylindrical/tube/fan/plate/pinnate/encrusting/other)	<2	3 & 4	5 & 6	7 & 8	9 – 10
Height (Visual estimate of average height of habitat architecture) (cm)	0-9	10-19	20-39	40-79	>10
Refuge size categories (Holes or gaps in habitat architecture or substratum in the following size categories 1-0, 6-15, 16,30, 31-50 and >50 cm)	0-1	2	3	4	5
Live cover (Total per cent cover of e.g., living corals, mangrove roots, seagrass, macroalgae and sponges)	0-19	20-39	40-59	60-79	80-100
Hard substratum (%)	0-19	20-39	40-59	60-79	80-100

3.4 Friction factor (RQ 3)

To obtain the friction factor (C_f) on the separate locations, first the bed shear stress was calculated and then used for obtaining the friction factor. Two different methods were used to calculate the bed shear stress: 1) using the Reynolds stress profile and 2) using the logarithmic velocity profile. The results from these two methods were then compared to get the best estimations of the friction factor.

Reynolds stress profile

To obtain the bed shear stress from the ADCP measurements using the Reynolds stress profile, the method of Tarya et al. (2010) was followed. In this method, a linear depth profile of the Reynolds stress is expected, with the Reynolds stress increasing from the surface to the bottom. However, in practice the linearity is not observed close to the bottom. To still obtain the bed shear stress, only the linear part of the Reynolds stress profile was used. The linear part of the Reynolds stress profile was determined with a visual assessment of the profile. When the linear fit was determined, it was extrapolated to the bed to obtain the bed shear stress. The Reynolds stresses were obtained from the ADCP measurements using Equation (1) and (2)

$$\overline{u'w'} = \frac{\overline{u_3^2} - \overline{u_4^2}}{4 \sin \theta \cos \theta} \quad (1)$$

$$\overline{v'w'} = \frac{\overline{u_1^2} - \overline{u_2^2}}{4 \sin \theta \cos \theta} \quad (2)$$

Where, the overbars denote the time averages, the primes the fluctuations from the average and θ the angle between the ADCP beams and central instrument axis ($^\circ$). In the equations, u_1 , u_2 , u_3

and u_4 represent the velocity components of the four beams (m/s). These were rotated in the way that u_3 and u_4 lie in the same plane as U (the long shore velocity component) and u_1 and u_2 lie in the same plane as V (the cross-shore velocity component).

The ADCP measurements were time averaged over periods of one hour for the Reynolds stress calculations.

Logarithmic velocity profile

From the averaged ADCP measurements, a depth velocity profile was expected. This profile was described using the law of the wall (Equation 3).

$$u = \frac{u_*}{k} \ln \frac{z}{z_0} \quad (3)$$

Where k is the Von Karmen constant ($= 0,4$), u_* the shear velocity (m/s), z the depth (m), and z_0 the roughness length (m). Using this equation, a depth velocity profile was fitted through the ADCP data. Then, when the roughness length determined from the velocity profile fit, the shear velocity (u_*) could be determined. The bed shear stress is then obtained using Equation (4) (Wilcock, 1996):

$$\tau_b = \rho * u_*^2 \quad (4)$$

With the calculated bed shear stresses from both methods, the friction factors could then be calculated using Equation (5)

$$C_f = \frac{\tau_b}{\rho U^2} \quad (5)$$

With τ_b , the bed shear stress (kg/ms²), ρ (kg/m³), the water density and U the water velocity (m/s). Due to the low flow velocities at the measurement sites, the data used for the two different methods were filtered to hours where the flow velocity was highest. The friction factor was then calculated using the average water velocity of these hours.

4. Results

4.1 Mean currents (RQ1)

The moored ADCP (together with the transect measurements) give an overview of the currents in shallow coastal areas. During all measurements, current velocities were below 0.1 m/s, only on a few occasions currents up to 0.2 m/s were measured. Due to these low velocities, patterns in the currents (temporal and over depth) are hard to distinguish. Figure 5a shows an example of the first measurement at Bsc Beach, where the velocities are hourly averaged. The Figure shows a high peak in velocity around 1-2 meters depth. This signal is probably caused by interference in one of the beams. This occurred in both the Bsc Beach measurements and at 1000 Steps. These peaks in velocity have not been taken into account in the analyses. An overview for the results of each measurement is given in Appendix 8.3.

No significant tidal currents were detected at any of the measurements. Figure 5b shows the depth averaged velocities and the tidal cycle with the changing water depth. Similar results were found in the other measurements, namely, that the currents did not seem to be affected by the tide. Also, for the locations where the two measurements were done around spring and neap tide, no clear changes were found in the currents. At Park Tului and Jeff Davis, higher velocities were measured during the spring tide measurement than during the neap tide measurement (see Appendix 8.3). However, if this would have been caused by the diurnal tide present at Bonaire, the velocities

would be stronger in two directions over the measurement period, for low and high tide. This is not the case, the increase in velocity during spring tide is in the same direction for the entire measurement. It is therefore likely that the spring-neap cycle did not cause this increased velocity.

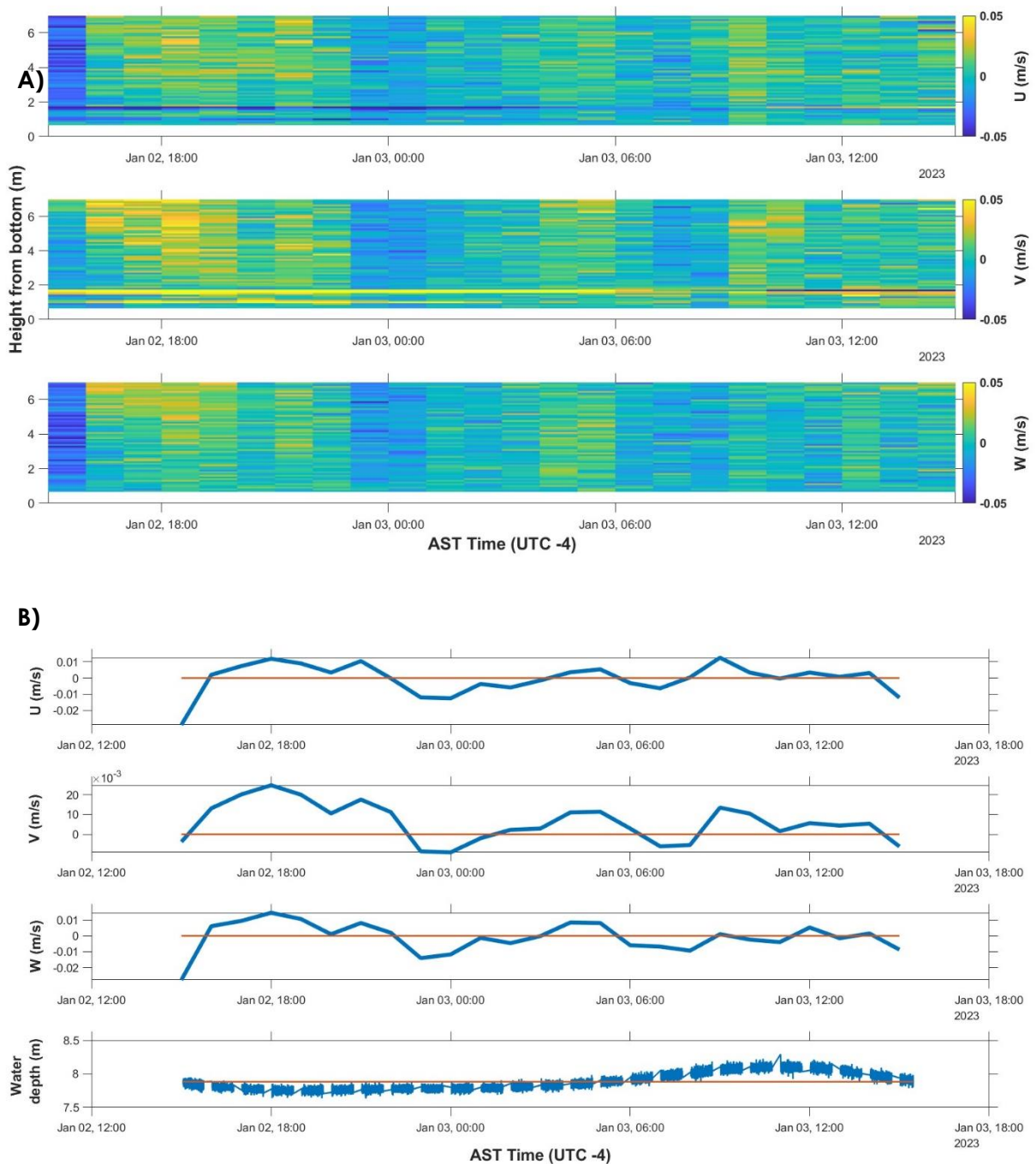


Figure 5: A) hourly averaged longshore (U), cross-shore (V) and vertical (W) velocity over time for the first Bsc Beach measurement, with positive numbers in the northward, offshore and upward direction B) Hourly and depth averaged longshore, cross-shore and vertical velocity and the water height from the bottom over time for the first Bsc Beach measurement.

A more likely explanation for this could be the weather circumstances during the measurements. Due to the absence of clear large-scale currents and tidal signals, it is likely that forcing by the wind can be important in driving the shallow water currents. During all the measurements, there generally was an easterly wind, with maximum variations north and south of maximum 32° and 27°

respectively. Figure 6 shows the relation between the average longshore current and the wind speed during each measurement. There is a clear correlation between the current velocity and the wind speed, with an r^2 of 0.83. Here, the discussed changes in current velocity between the two measurements at Park Tului and Jeff Davis are clearly visible. Also, the absence of this at Bsc Beach could be explained by the fact that there was barely a difference in wind speed between the two measurement days. 1000 Steps is the only measurement that does not follow the observed correlation between the wind and the longshore current.

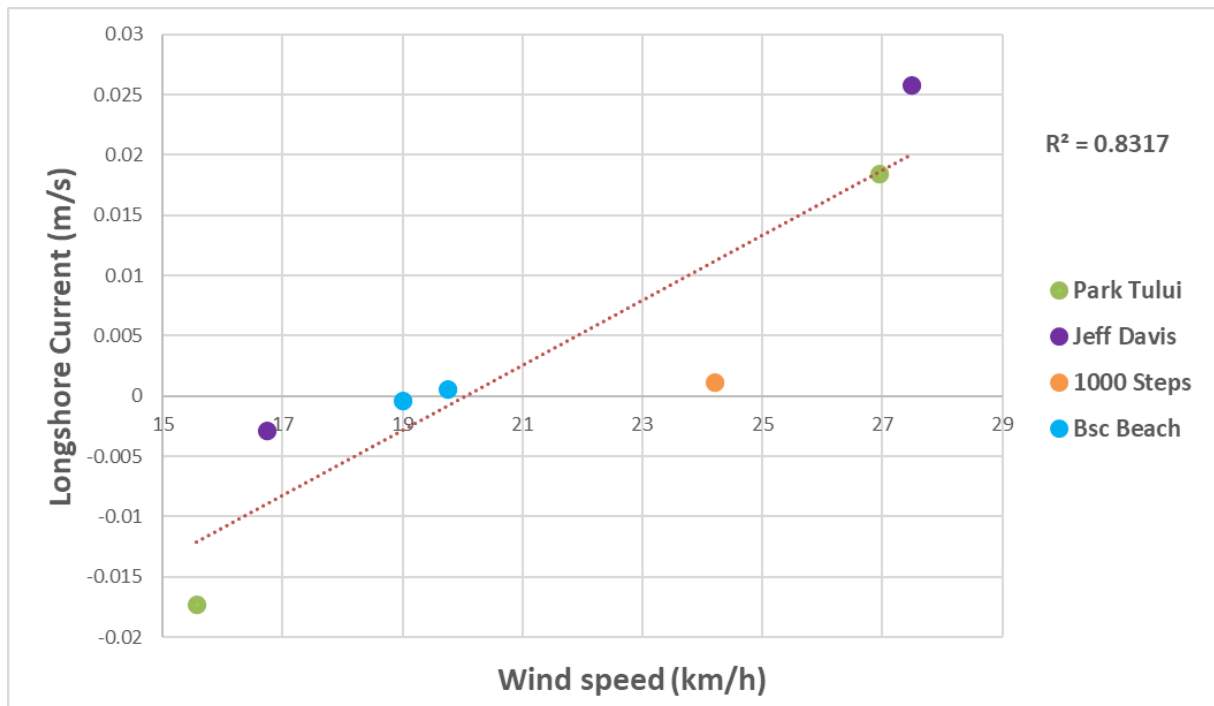


Figure 6: Longshore velocities compared to the wind speed for all measurements (wind speeds: Meteostat.net, 2023)

During periods of stronger currents along the coast, a response in the vertical velocity was observed on most occasions. Stronger northward currents generally resulted in an upward vertical velocity. This happened at Park Tului 07-02 (Appendix 8.3.1, right side) and at Bsc Beach 02-01 (Figure 5). Contrary, stronger southward currents resulted in a downward vertical velocity at 1000 Steps (Appendix 8.3.4). To ensure that these correlations were not caused by a strong tilt of the ADCP during the measurements, the vertical component of the longshore current ($U \cdot \cos(\text{tilt})$), caused by the tilt, was compared to the vertical velocity. The tilt was for all measurements between the $0-8^\circ$, with all except Bsc Beach being between $0-4^\circ$. The resulting velocities were around one order of magnitude smaller than the measured vertical velocities. This indicates that the tilt of the ADCP measurement does not completely explain the correlation between the longshore and vertical velocity during periods of stronger currents.

4.2 Rugosity (RQ2)

The three different methods to assess the reef health / reef rugosity rendered almost identical results. Table 3 shows the results for the two rugosity analysis methods and the HAS-score for every location (for the 3-D models and DEM of all locations, see Appendix 8.2). The expected changes in reef rugosity between the locations, an increase in rugosity with live coral presence, are observed both with the rugosity transects and the virtual chain method. The results of the two methods showed an r^2 of 0.98 in their correlation. These results are very well in line with the visual

assessment of the reef health (the HAS-score). The HAS-score had an r^2 of 0.97 and 0.99 with the results of the rugosity transects and the virtual chain method, respectively.

Table 3: Results of the rugosity analyses and reef health assessment

<i>Location</i>	<i>Rugosity transects standard deviation (m)</i>	<i>Virtual chain method (3D-model) ratio</i>	<i>HAS-score</i>
Park Tului	0.02	1.05	1.1
Bsc Beach	0.16	1.41	2.7
Jeff Davis	0.28	1.58	3.1
1000 Steps	0.47	1.90	4.5

The fact that the measured rugosity corresponds so closely with the visual assessment of the reef health shows that the rugosity in these areas is strongly determined by the coral structures. The live corals create hard structures that give the strongest height variation on the sea floor. Also, in the Park Tului area, where the sea floor is near flat, previous rugosity of coral structures, alive or dead, are now less pronounced due to sedimentation that has reduced rugosity in this area around Kralendijk.

4.3 Friction factor (RQ3)

To assess the relation between the rugosity and the turbulent mixing over the shallow reef areas, the friction factor was calculated at all locations (Figure 7). The results for the Bsc Beach longshore and Jeff Davis longshore and cross-shore measurements are omitted, because no logarithmic fit could be made to the velocity profile. For the other method, the results for the longshore measurements at the Bsc Beach 1 and Jeff Davis 1 measurements, as well as the cross-shore measurement for the Jeff Davis 2 measurement, were omitted for the same reason. Figure 7 show a clear difference in the calculated friction factors between the logarithmic velocity profile fit method (Figure 7a) and the Reynolds stress depth profile fit method (Figure 7b). The results using the logarithmic velocity profile resulted in more realistic results, with the friction factor ranging from 0 to 0.6. The second method, using the Reynolds stress profile, resulted in remarkably high and low values, up to -14 for the friction factor. As these were several orders of magnitude larger than expected, they were considered unrealistic and only the results of the first method were used for comparison.

From the results there is no clear relation visible between the friction factor and the reef rugosity. Both high rugosity areas (Jeff Davis and 1000 Steps) do show high friction factors. However, these are not higher than the friction factor found at Park Tului, during the first measurement. Park Tului 1 and Jeff Davis 2 show a higher friction factor for the longshore direction, but this is not likely related to the rugosity as Park Tului is a low rugosity area and Jeff Davis a high rugosity area (see Table 3). They are, however, two measurements with a strong average current. Park Tului 2 on the other hand, also has a strong average current but has a much smaller friction factor. For the cross-shore direction there does seem to be a difference in friction factor and the rugosity. Here, Park Tului and Bsc Beach show low friction factors and Jeff Davis and 1000 Steps show high friction factors. However, the relation cannot be confirmed with certainty, due to the high uncertainty, especially for the Jeff Davis measurement.

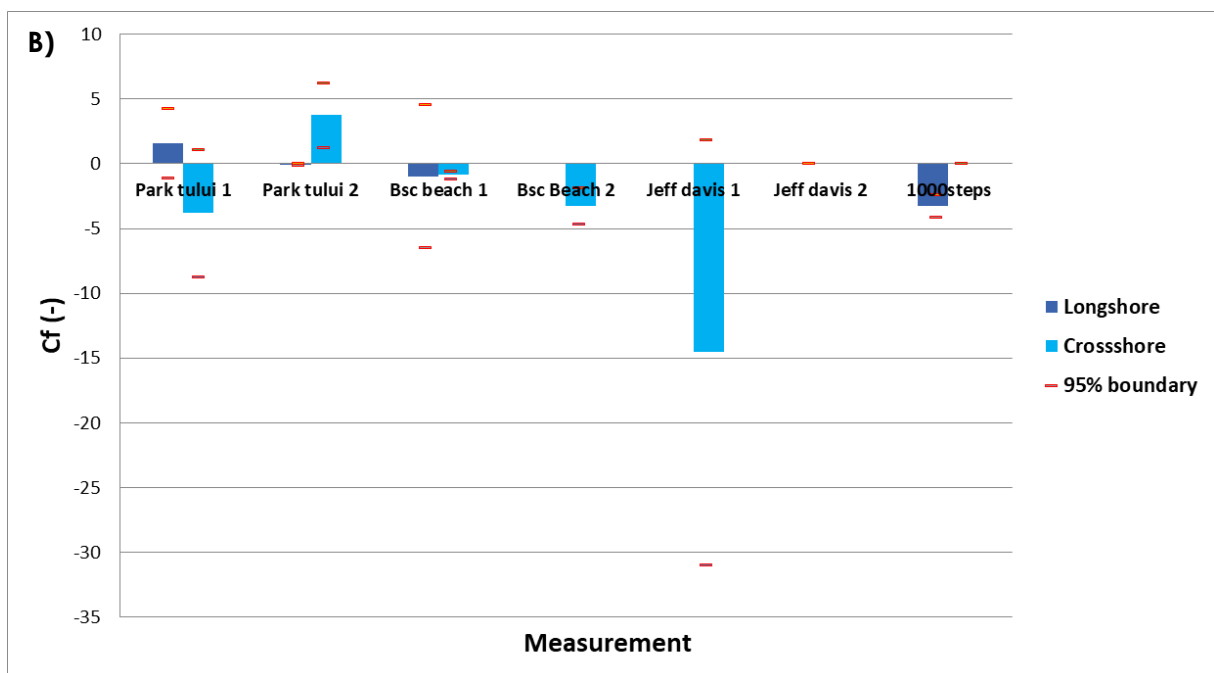
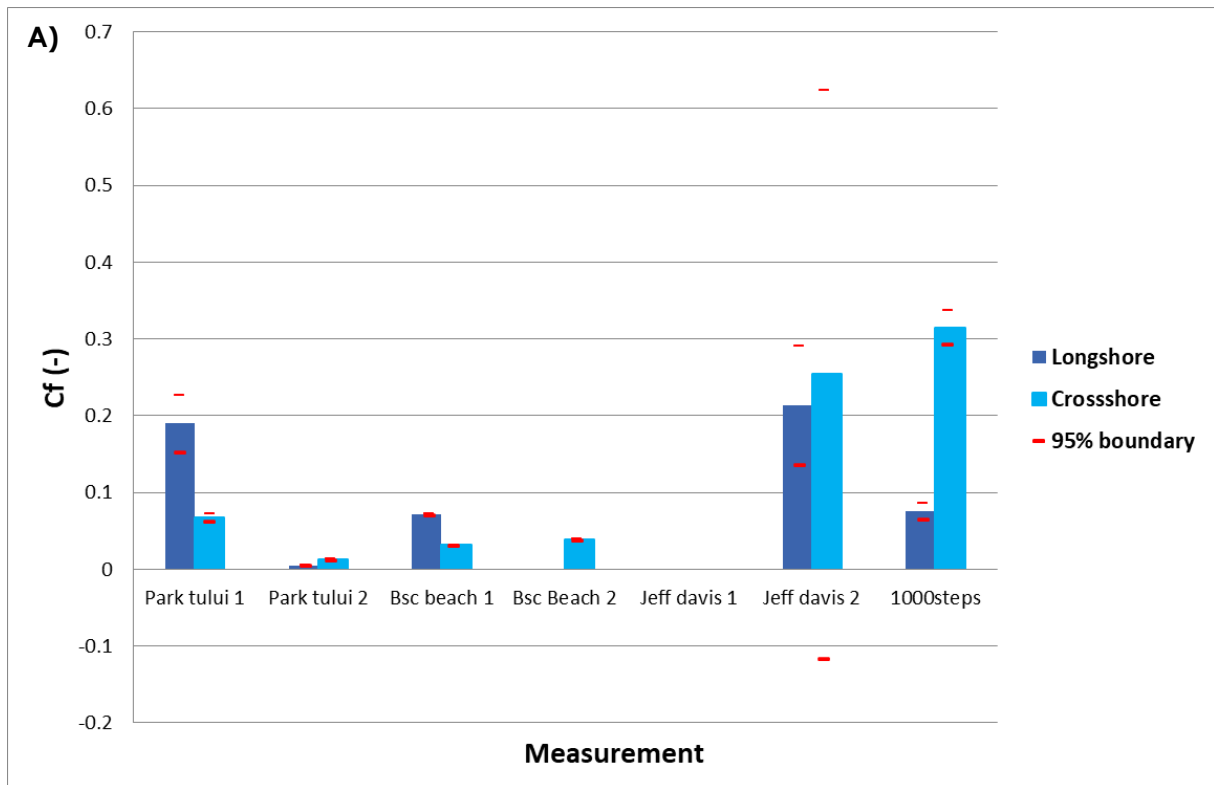


Figure 7: Friction factor (C_f) with 95% boundary A) derived from the logarithmic velocity profiles and B) from the Reynolds stress depth profiles. The scales differ from -0.2-0.7 for the method using the logarithmic velocity profile to -200-50 for the method using the Reynolds stress profile, due to the high numbers calculated with the Reynolds stress profile.

Furthermore, a large difference in the alongshore friction factor is observed between the two measurements at Park Tului. This difference in friction factor comes together with a difference in flow velocity between the measurements as well. The first measurement had a low average velocity, but shows a high friction factor, whereas the second measurement had a high average velocity, but a low friction factor. This difference in friction factor is not reflected in the cross-shore direction, but there was also no large difference in average cross-shore flow velocity between the

sites. This seems only to occur at Park Tului, because Jeff Davis shows high friction factors in both the longshore and cross-shore direction despite a high flow velocity.

5. Discussion

5.1 Currents (RQ 1 & 3)

The analyses of the coastal currents showed low flow velocities all along the coast. A minimal average northward current was observed. The cross-shore currents showed no consistent patterns and no tidal signal, neither diurnal nor spring-neap cycles, could be distinguished in the data. The relation with the constant offshore wind and the longshore current showed that wind forcing is likely to be the most important driver of the coastal currents. These wind-driven currents did not seem to be affected by the reef rugosity, as the results are similar for locations with high and low rugosity. The friction factors found seemed to show an increase with higher rugosities for the cross-shore direction. However, there was a high uncertainty in the calculated friction factors, especially for the method using the Reynolds stress profiles.

In the average currents measured along the coast, the counter rotating currents in the island wake as described by Wolanski (1984) were not observed. According to the Wolanski model, longshore currents in the north and the south would flow into opposite directions. The observed average currents were, however, either near zero or directed towards the north, with the exception of the 31-01 Park Tului measurement. The general northward current is in line with the results of Van Leeuwen (2022), who measured the currents along the coast up to 40 meters depth along the west coast of Bonaire. An explanation for the absence of the two counter rotating eddies could be that the south side of Bonaire lies perpendicular to the large-scale westward current around the island, whereas the north side lies directed to the north-west, more along the current. This could result in a stronger counter rotating eddy in the south than in the north, and therefore a stronger northward current. Another explanation could be the presence of Klein Bonaire, which could act as an interference for the counter rotating currents, also resulting in a slower average current. Lastly, the constant easterly wind at Bonaire could also favour northward currents. The wind forcing could induce a current deflected to the north, due to the Ekman spiral (Dritschel, 2020). This is strengthened by the fact that the strong correlation between the longshore current and the wind speed (Figure 6) suggests that the currents are driven primarily by the wind. Van Duyl (1985) and Van Leeuwen (2022) reported a similar situation, based on the lack of a strong wave and tidal forcing. The fact that the longshore current at 1000 Steps had a worse correlation with the wind could have multiple explanations. First of all, it could be that there are other factors influencing the currents in that area, which decreases the influence of the wind. Secondly, the wind data used are collected at the Flamengo airport, close to Bsc Beach, which makes 1000 Steps the furthest measurement location from this weather station. This could mean that the wind may have been different at 1000 Steps. And lastly, 1000 Steps is located in front of the more mountainous part of Bonaire compared to the other locations, which could mean that this location is more sheltered from the wind, especially close to the coast. As a result, it could be that the wind speed around the location of the ADCP was actually lower than recorded by the weather station. Reef rugosity, on the other hand, did not seem to affect the changes in longshore velocity as caused by changes in wind speed. Both at Park Tului (low rugosity) and Jeff Davis (high rugosity) similar changes in the wind strength resulted in similar changes in the cross-shore flow velocity.

During periods of stronger longshore currents, a response in the vertical current was observed on multiple occasions. When the longshore current was stronger in the northward direction at Park

Tului and Bsc Beach (see Appendix 8.3.1 and 8.3.2) an upward current (upwelling) was reported. Similarly, when a stronger southward current was present at Park Tului and 1000 Steps (see Appendix 8.3.1 and 8.3.4) a downward current (downwelling) was observed. This was different than the expected response, where a northward current would be deflected to right (onshore) resulting in downwelling due to an Ekman boundary layer (Hoitink, 2003). Similarly, upwelling would be expected with a southward current. The correlation was also not likely caused by measuring errors due to an ADCP tilt. The vertical velocity components of the longshore current, caused by a tilt of the ADCP, were in all cases at least one order of magnitude smaller than the vertical velocity. This makes it unlikely that the correlation between the longshore and vertical current can be explained by a tilt of the ADCP during the measurement. An explanation for this could be that an offshore wind created an offshore current, resulting in upwelling (Kämpf, 2017). However, this would not explain the downwelling at 1000 Steps, because an easterly wind was present there as well. The question to what causes this change in balance for upwelling and downwelling, could be inspiration for further research.

5.2 Rugosity and friction factor (RQ 2 & 3)

The two methods used for calculating the friction factor, based on earlier studies from Tarya et al. (2010) and Wilcock (1996), gave strongly differing results. The results using the logarithmic velocity profiles, from Wilcock (1996), were thought to be more accurate than the method using the Reynolds stress profiles, from Tarya et al. (2010), for two main reasons: firstly, the friction factors calculated showed numbers of the same order of magnitude as other studies reporting friction factors in coral reef areas (Lugo-Fernandez et al., 1998; Wolanski & Thomson, 1984; Van Dongeren et al., 2012; Ribes & Atkinson, 2007). Secondly, the low flow velocities at all locations increased the error by noise, especially for the Reynolds stress profile method. Because the Reynolds stresses are calculated before being averaged over a one-hour period, the increased influence of noise at low velocities results in larger errors in this method compared to the logarithmic velocity profile method (Zhu et al., 2016). This could explain the large difference between the two methods.

The friction factors calculated with the logarithmic velocity profiles did not show a clear connection with the reef rugosity at the locations. A trend of increased friction factors with increased rugosity was visible, but this could not be concluded with certainty due to the high error margins on the friction factors. The increased friction factors are in this case likely caused by the rugosity, because the cross-shore velocities are similar for all locations, between 0.0036 and 0.0059 m/s. Whether this would result in stronger mixing in high rugosity areas cannot be concluded with certainty, because for turbulence to be generated from bottom friction the water has to move over the reef. However, the velocities in the cross-shore direction may too low to do this effectively. If velocities would increase, this could result in increased turbulence in the high rugosity areas and improve vertical mixing (Bergquist & Boyle, 2006; Chase et al., 2005; Cole et al., 1985; Dunckley et al., 2012; Hearn, 1999). An important note here is that increased friction under higher current velocities will also slow down the general current in its turn, and therefore decrease the mixing again. Lim et al. (2020) point out that, under higher flow velocities, there will not necessarily be more vertical mixing over the water column, but that transfer of particles into the reef areas may be increased due to the increased turbulence and the deceleration of the current. Mixing over the water column is, however, not only dependent on the bottom friction, but on the current velocity as well. Here, the relation of the wind and longshore current suggest that the current velocities are not strongly influenced by the reef rugosity. It was shown that similar changes in wind forcing resulted in similar changes in water velocity for high and low rugosity areas. So, this could mean that in some cases

of stronger wind forcing increased turbulence from bottom friction will occur in high rugosity areas, while the general current is not strongly affected, thus potentially resulting in stronger vertical mixing.

The results of this research suggest that nutrients entering the coastal waters on the west side of Bonaire are not transported away by strong currents, due to the low average velocities all along the coast. The absence of tidal forcing and cross-shore currents increase the likelihood that nutrients stay in the coastal area and can enter the coral reefs. No strong evidence for increased mixing over high rugosity areas compared to low rugosity areas has been found to support an increased nutrient mixing over coral reefs compared to sandy/rubble areas. The evidence of the wind domination in coastal currents do suggest that during periods of stronger wind forcing an increased mixing of nutrients can occur and potentially stronger over high rugosity areas, because stronger currents will result in an increased bottom friction and therefore turbulence, potentially stronger in high rugosity areas, as the currents forced by the wind did not seem affected by the reef rugosity. It is then also important to note that, considering that wind is an important forcing for the velocities and the mixing, that events of high nutrient input are often accompanied by stormy weather with heavy precipitation and intense winds, thus aggravating the effects.

This research has pointed to dominance of the wind as the forcing factor of water movement in the shallow coastal zone of west Bonaire. The calculated friction factors did not show consistent patterns between the different measurement sites, due to low average velocities. As a result, the calculation of the friction factor were only based on logarithmic fits to the velocity profiles with low coefficients of determination (r^2), ranging between 0.23 and 0.53. This makes that the relations found in this research cannot be taken as scientific proof but rather as indications and inspiration for further research. Furthermore, during this research the role of waves has not been taken into account. Due to the reported low wave climate on the west coast, it was assumed less influential than tidal motion and wind forcing (van Duyl, 1985). However, with an absence of strong tidal currents, wave forcing could be a more important factor in nutrient flow in the shallow coastal waters, especially during times of low wind forcing. Also, considering the fact that nutrient inflow due to rain events is a large part of the total nutrient supply, the role of freshwater input on the coastal hydrodynamics is important for local nutrient transport (Moum & Smyth, 2001). Especially considering that rain events are often accompanied by increased wave and wind forcing, increasing the mixing. Furthermore, there are other factors that should be considered when looking at nutrient transport in the coastal zone. Mixing in these areas is often also dependent on density stratification of the water, which may promote or obstruct mixing (Monismith et al., 2018). This may be an even more important factor considering that the flow velocities are low and that this might limit turbulent mixing.

6. Conclusion

The sheltered situation on the west side of Bonaire makes it a coastal zone, with little forcing from large scale currents and wave forcing. Due to the microtidal circumstances in the area, tidal currents are negligible in the shallow waters. Influence of the wind, on the other hand, was clearly measured, showing that stronger easterly winds resulted in higher cross-shore velocities, and often also stronger longshore velocities. The longshore currents, forced by the wind, were not affected by coral reef presence in the shallow areas, as changes in wind velocity resulted in similar changes in cross-shore velocity for both areas with high rugosity and low rugosity. In terms of mixing, the changes in velocity might result in a different response with reef rugosity. The friction factor data suggested a weak relation with reef rugosity. This does not have to result in an increased mixing over the water column, but during higher flow velocity periods, it could lead to increased trapping of nutrients in coral reefs, due to increased turbulence around the coral reefs and a deceleration of the current. In the present research are the effects of stratification on the mixing over depth and the input of nutrient rich fresh water during rain events have not been taken into account. These aspects which could lead to a different nutrient distribution and may therefore be important in the nutrient supply in coastal coral reefs and could therefore be interesting future research topics.

6.1 Acknowledgements

This research was conducted for Wageningen University under the INREEF project and WMR, with support from STINAPA during the fieldwork, with a special thanks to Bart Vermeulen and Roxanne-Liana Fransisca for their supervision and support both during my time in Wageningen and the Fieldwork on Bonaire. I would also like to thank all my co-divers and who helped me during the measurements and Dive Friends and STINAPA who provided boats for this research. Lastly, I would like to thank Noémie Bernardin for her continuous support and feedback during this project.

7. References

- Bergquist, B. A., & Boyle, E. A. (2006). Iron isotopes in the Amazon River system: Weathering and transport signatures. *Earth and Planetary Science Letters*, 248(1–2), 54–68. <https://doi.org/10.1016/j.epsl.2006.05.004>
- Bremer, T. S. Van Den, & Breivik, O. (2018). Stokes drift. 376(2111), 1–23.
- Burchard, H., Craig, P. D., Gemmrich, J. R., van Haren, H., Mathieu, P. P., Meier, H. M., ... & Wijesekera, H. W. (2008). Observational and numerical modeling methods for quantifying coastal ocean turbulence and mixing. *Progress in oceanography*, 76(4), 399–442.
- Chase, Z., Hales, B., Cowles, T., Schwartz, R., & van Geen, A. (2005). Distribution and variability of iron input to Oregon coastal waters during the upwelling season. *Journal of Geophysical Research C: Oceans*, 110(10), 1–14. <https://doi.org/10.1029/2004JC002590>
- Clean Water Team (CWT). (2004). Electrical conductivity/salinity fact sheet, FS-3.1.3.0(EC). Clean Water Team Guidance Compendium for Watershed Monitoring and Assessment State Water Resources Control Board, Version 2.0., 0, 2–6.
- Cole, K. H., Guinasso, N. L., Richardson, M. D., Johnson, J. W., & Schink, D. R. (1985). Uranium and thorium series isotopes in recent sediments of the Venezuela Basin, Caribbean Sea. *Marine Geology*, 68(1–4), 167–185. [https://doi.org/10.1016/0025-3227\(85\)90010-6](https://doi.org/10.1016/0025-3227(85)90010-6)
- Courtney, T. A., & Andersson, A. J. (2019). Evaluating measurements of coral reef net ecosystem calcification rates. *Coral Reefs*, 38(5), 997–1006. <https://doi.org/10.1007/s00338-019-01828-2>
- Davis, K. A., Pawlak, G., & Monismith, S. G. (2021). Turbulence and Coral Reefs. *Annual Review of Marine Science*, 13, 343–373. <https://doi.org/10.1146/annurev-marine-042120-071823>
- de Bakker, D. M., Meesters, E. H., Bak, R. P. M., Nieuwland, G., & van Duyl, F. C. (2016). Long-term shifts in coral communities on shallow to deep reef slopes of Curaçao and Bonaire: Are there any winners? *Frontiers in Marine Science*, 3(NOV), 1–14. <https://doi.org/10.3389/fmars.2016.00247>
- DeCarlo, T. M., Gajdzik, L., Ellis, J., Coker, D. J., Roberts, M. B., Hammerman, N. M., Pandolfi, J. M., Monroe, A. A., & Berumen, M. L. (2020). Nutrient-supplying ocean currents modulate coral bleaching susceptibility. *Science Advances*, 6(34). <https://doi.org/10.1126/sciadv.abc5493>
- Dritschel, G. D., Paldor, N., & Constantin, A. (2020). The ekman spiral for piecewise-uniform viscosity, 16, 1089–1093. <https://doi.org/10.5194/os-16-1089-2020>
- Dunckley, J. F., Koseff, J. R., Steinbuck, J. V., Monismith, S. G., & Genin, A. (2012). Comparison of mixing efficiency and vertical diffusivity models from temperature microstructure. *Journal of Geophysical Research: Oceans*, 117(10), 1–12. <https://doi.org/10.1029/2012JC007967>
- Dustan, P., Doherty, O., & Pardede, S. (2013). Digital Reef Rugosity Estimates Coral Reef Habitat Complexity. *PLoS ONE*, 8(2), 1–10. <https://doi.org/10.1371/journal.pone.0057386>
- Edmunds, P. J., & Burgess, S. C. (2018). Colony size and turbulent flow speed modulate the calcification response of the coral *Pocillopora verrucosa* to temperature. *Marine Biology*, 165(1), 1–12. <https://doi.org/10.1007/s00227-017-3257-z>
- Engel, M., Br, H., Scheffers, S., Wennrich, V., & Kelletat, D. (2012). Shoreline changes and high-energy wave impacts at the leeward coast of Bonaire (Netherlands Antilles). 905–921. <https://doi.org/10.5047/eps.2011.08.011>
- Hearn, C. J. (1999). Wave-breaking hydrodynamics within coral reef systems and the effect of

- changing relative sea level. *Journal of Geophysical Research: Oceans*, 104(C12), 30007–30019. <https://doi.org/10.1029/1999jc900262>
- Hearn, C. J. (2011). Perspectives in coral reef hydrodynamics. *Coral Reefs*, 30(SUPPL. 1), 1–9. <https://doi.org/10.1007/s00338-011-0752-4>
- Hoitink, A. J. F. (2003). Physics of coral reef systems in a shallow tidal embayment. In *Nederlandse Geografische Studies (Issue 313)*.
- Hyee, S. L., Alex, F., & Antony, M. K. (2020). Spatial arrangement of biogenic reefs alters boundary layer characteristics to increase risk of microplastic bioaccumulation, 15(6). <https://doi.org/10.1088/1748-9326/ab83ae>
- Hylkema, A., Vogelaar, W., & Meesters, H. W. G. (2015). Fish Species Utilization of Contrasting sub-Habitats Distributed Along an Ocean-to-Land Environmental Gradient in a Tropical Mangrove and Seagrass Lagoon. 1448–1465. <https://doi.org/10.1007/s12237-014-9907-1>
- meteostat.net. (2023). Flamingo Airport, Bonaire. Retrieved from [meteostat.net: https://meteostat.net/nl/station/78990?t=2023-01-19/2023-01-20](https://meteostat.net/nl/station/78990?t=2023-01-19/2023-01-20)
- Kämpf, J. (2017). Wind-Driven Overturning, Mixing and Upwelling in Shallow Water: A Nonhydrostatic Modeling Study. *Journal of Marine Science and Engineering*, 2017, 5, 47. <https://doi.org/10.3390/jmse5040047>
- Lugo-Fernandez, A., Roberts, H. H., Wiseman Jr, W. J., & Carter, B. L. (1998). Water level and currents of tidal and infragravity periods at Tague Reef, St. Croix (USVI). *Coral Reefs*, 17, 343-349.
- Monismith, S. G. (2007). Hydrodynamics of coral reefs. *Annual Review of Fluid Mechanics*, 39, 37–55. <https://doi.org/10.1146/annurev.fluid.38.050304.092125>
- Monismith, S. G., Koseff, J. R., & White, B. L. (2018). Mixing efficiency in the presence of stratification: When is it constant?. *Geophysical Research Letters*, 45(11), 5627-5634.
- Moody, L. F., Princeton, N.J. (1944). Friction factors for pipe flow. *Transactions of the American Society of Mechanical Engineers*, 66(8), 671-678.
- Morais, R. A., Depczynski, M., Fulton, C., Marnane, M., Narvaez, P., Huertas, V., Brandl, S. J., & Bellwood, D. R. (2020). Severe coral loss shifts energetic dynamics on a coral reef. *Functional Ecology*, 34(7), 1507–1518. <https://doi.org/10.1111/1365-2435.13568>
- Moum, J. N., & Smyth, W. D. (2001). Upper ocean mixing. *Encyclopedia of Ocean Sciences*, 6, 3093-3100.
- Mucher. (2016). Coral Reef Bonaire. <https://www.dcbd.nl/document/hyperspectral-coral-reef-classification-bonaire>
- Osorio-Cano, J. D., Alcérreca-Huerta, J. C., Mariño-Tapia, I., Osorio, A. F., Acevedo-Ramírez, C., Enriquez, C., Costa, M., Pereira, P., Mendoza, E., Escudero, M., Astorga-Moar, A., López-González, J., Appendini, C. M., Silva, R., & Oumeraci, H. (2019). Effects of Roughness Loss on Reef Hydrodynamics and Coastal Protection: Approaches in Latin America. *Estuaries and Coasts*, 42(7), 1742–1760. <https://doi.org/10.1007/s12237-019-00584-4>
- Petrie, J., Diplas, P., Gutierrez, M., & Nam, S. (2013). Combining fixed- and moving-vessel acoustic Doppler current profiler measurements for improved characterization of the mean flow in a natural river. *Water Resources Research*, 49(9), 5600–5614. <https://doi.org/10.1002/wrcr.20396>
- Ribes, M., & Atkinson, M. J. (2007). Effects of water velocity on picoplankton uptake by coral reef communities. *Coral Reefs*, 26, 413-421.

- Rogers, J. S., Maticka, S. A., Chirayath, V., Woodson, C. B., Alonso, J. J., & Monismith, S. G. (2018). Connecting flow over complex terrain to hydrodynamic roughness on a coral reef. *Journal of Physical Oceanography*, 48(7), 1567–1587. <https://doi.org/10.1175/JPO-D-18-0013.1>
- Sandin, A., Stuart, A., & Eugenia, M. (2008). Coral reef fish and benthic community structure of Bonaire and Curaçao , Netherlands Antilles. 44(2), 137–144.
- seatemperatu.re. (2023). Tide schedule in Bonaire (Netherlands Antilles). Retrieved from seatemperatu.re: <https://www.seatemperatu.re/caribbean/netherlands-antilles/bonaire/tides/month/october/>
- Stocking, J. B., Laforsch, C., Sigl, R., & Reidenbach, M. A. (2018). The role of turbulent hydrodynamics and surface morphology on heat and mass transfer in corals. *Journal of the Royal Society Interface*, 15(149). <https://doi.org/10.1098/rsif.2018.0448>
- Stokes, Leichter, & Genovese. (2010). Long-Term Declines in Coral Cover At Bonaire , Netherlands Antilles. *Atoll Research Bulletin*, 582.
- Tarya, A., Hoitink, A. J. F., & Van Der Veegt, M. (2010). Tidal and subtidal flow patterns on a tropical continental shelf semi-insulated by coral reefs. *Journal of Geophysical Research: Oceans*, 115(9), 1–16. <https://doi.org/10.1029/2010JC006168>
- Teneva, L., Dunbar, R. B., Mucciarone, D. A., Dunckley, J. F., & Koseff, J. R. (2013). High-resolution carbon budgets on a Palau back-reef modulated by interactions between hydrodynamics and reef metabolism. *Limnology and Oceanography*, 58(5), 1851–1870. <https://doi.org/10.4319/lo.2013.58.5.1851>
- Thomas, F. I. M., & Atkinson, M. J. (1997). Ammonium uptake by coral reefs: effects of water velocity and surface roughness on mass transfer. *Limnology and Oceanography*, 42(1), 81–88.
- Van Dongeren, A. P., Lowe, R., Pomeroy, A., Trang, D. M., Roelvink, D., Symonds, G., & Ranasinghe, R. (2013). Numerical modeling of low-frequency wave dynamics over a fringing coral reef. *Coastal Engineering*, 73, 178–190. <http://dx.doi.org/10.1016/j.coastaleng.2012.11.004>
- van Duyl, F. C. (1985). *Atlas of the Living Reefs of Curaçao and Bonaire (Netherlands Antilles) By Fleur.*
- Van Leeuwen, A. M. (2022). Assessing the Relationship between Coastal Currents and Water Quality Indicators on Bonaire : ADCP & CTD approach.
- Vanwonderghem, I., & Webster, N. S. (2020). Coral Reef Microorganisms in a Changing Climate. *IScience*, 23(4), 100972. <https://doi.org/10.1016/j.isci.2020.100972>
- Vermeulen, B. (2015). Adcptools: Set of functions to process acoustic Doppler current profiler data. <https://sourceforge.net/projects/adcptools/>
- Wilcock, P. R. (1996). Estimating local bed shear stress from velocity observations. *Water Resources Research*, 32(11), 3361–3366.
- Wolanski, E., Imberger, J., & Heron, M. L. (1984). Island wakes in shallow coastal waters. *Journal of Geophysical Research*, 89(C6), 10553. <https://doi.org/10.1029/jc089ic06p10553>
- Wolanski, E., & Thomson, R. E. (1984). Wind-driven circulation on the northern Great Barrier Reef continental shelf in summer. *Estuarine, Coastal and Shelf Science*, 18(3), 271–289.
- Woodhead, A. J., Hicks, C. C., Norström, A. V., Williams, G. J., & Graham, N. A. J. (2019). Coral

reef ecosystem services in the Anthropocene. *Functional Ecology*, 33(6), 1023–1034. <https://doi.org/10.1111/1365-2435.13331>

Zhu, Q., van Prooien, B.C., Wang, Z.B., Ma, Y.X., Yang, S.L. (2016). Bed shear stress estimation on an open intertidal flat using in situ measurements. *Estuarine, Coastal and Shelf Science*, 182 (2016) 190-201. <http://dx.doi.org/10.1016/j.ecss.2016.08.028>

8. Appendices

8.1 Rugosity and ADCP methods

8.1.1 Reference objects 3-D filming

<i>Reference Object</i>	<i>Size (cm)</i>
Measurement stick	150
Black and white striped stick	49
Measurement tape	26

8.1.2 ADCP settings overview + Commands

Table 4: ADCP procedures

<i>ADCP setting</i>	<i>value</i>	<i>unit</i>
Deployment time	1.1	days
Burst interval	1	Hours
Ensembles per burst	2218	-
Ensemble interval	0.85	seconds
Pings per ensemble	1 (3 sub-ping)	-
Depth cell size	0.1/0.2	meter

Table 5: Moored ADCP commands

Park Tului 31-01	Park Tului 07-02	Bsc Beach 02- 01	Bsc Beach 09- 01	Jeff Davis 16-01	Jeff Davis 06-02	1000 Steps 19- 01
CR1	CR1	CR1	CR1	CR1	CR1	CR1
WM12	WM12	WM12	WM12	WM12	WM12	WM12
CF111111	CF111111	CF111111	CF111111	CF111111	CF111111	CF111111
EA0	EA0	EA0	EA0	EA0	EA0	EA0
EB0	EB0	EB0	EB0	EB0	EB0	EB0
ED100	ED100	ED100	ED100	ED70	ED70	ED100
ES35	ES35	ES35	ES35	ES35	ES35	ES35
EX00000	EX00000	EX00000	EX00000	EX00000	EX00000	EX00000
EZ111110 1	EZ111110 1	EZ111110 1	EZ111110 1	EZ111110 1	EZ111110 1	EZ111110 1
WB0	WB0	WB0	WB0	WB0	WB0	WB0
WD111100 000	WD111100 000	WD111100 000	WD111100 000	WD111100 000	WD111100 000	WD111100 000
WF44	WF44	WF44	WF44	WF44	WF44	WF44
WN49	WN49	WN100	WN100	WN34	WN34	WN49
WP1	WP1	WP1	WP1	WP1	WP1	WP1
WS20	WS20	WS10	WS10	WS20	WS20	WS20
WO3,16	WO3,16	WO3,16	WO3,16	WO3,16	WO3,16	WO3,16
WV175	WV175	WV175	WV175	WV175	WV175	WV175
TE00:00:0 0.85	TE00:00:0 0.85	TE00:00:0 0.85	TE00:00:0 0.85	TE00:00:0 0.85	TE00:00:0 0.85	TE00:00:0 0.85

TP00:00.8 5	TP00:00.8 5	TP00:00.8 5	TP00:00.8 5	TP00:00.8 5	TP00:00.8 5	TP00:00.8 5
TB01:00:0 0:00	TB01:00:0 0:00	TB01:00:0 0:00	TB01:00:0 0:00	TB01:00:0 0:00	TB01:00:0 0:00	TF23/01/1 9 13:30:00
TC02118	TC02118	TC02118	TC02118	TC02118	TC02118	TB01:00:0 0:00
WA50	WA50	WA50	WA50	TF23/01/2 3 20:30:00	TF23/02/0 6 19:00:00	TC02118
TF23/01/3 1 20:00:00	TF23/02/0 7 22:00:00	TF23/01/0 2 15:15:00	TF23/01/0 9 15:15:00	WA50	WA50	WA50
CK	CK	CK	CK	CK	CK	CK
CS	CS	CS	CS	CS	CS	CS

8.2 3-D models + DEM

8.2.1 Park Tului

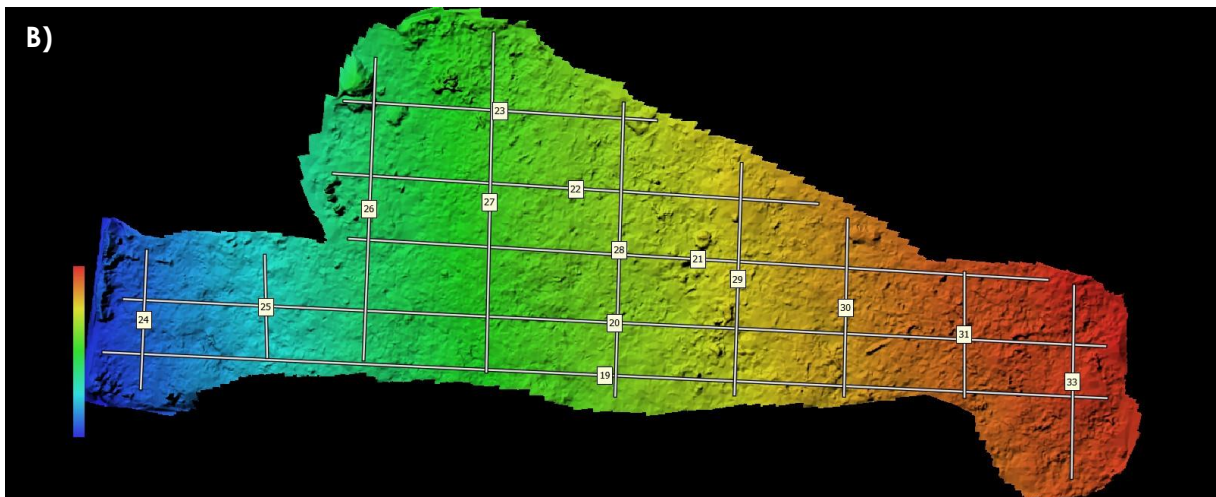
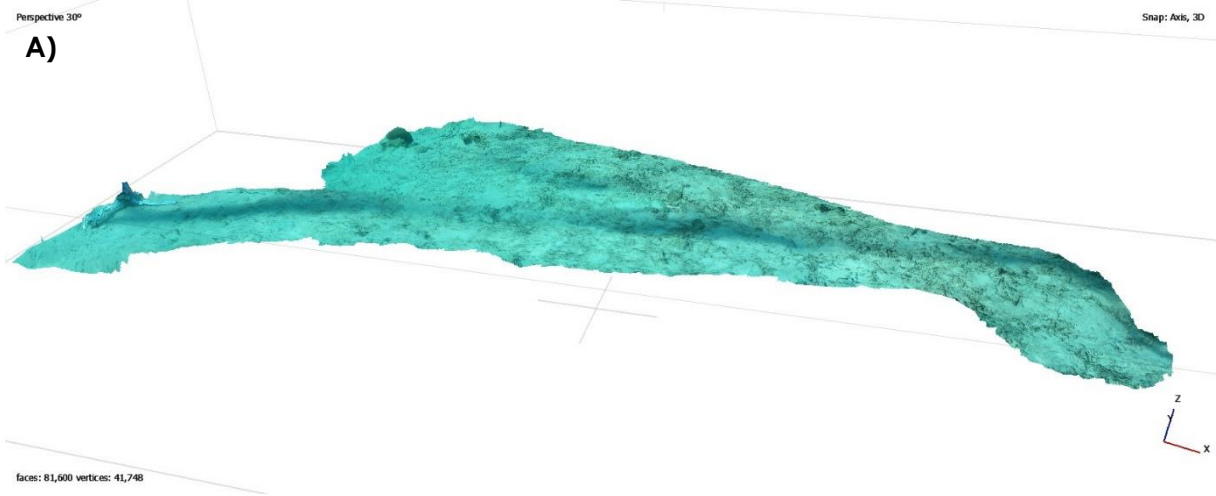


Figure 8: A) Metashape Agisoft generated 3-D model Park TULUI AND B) Metashape Agisoft generated DEM Park Tului, with the virtual chains used for the rugosity (Low → high is blue → red)

8.2.2 Bsc Beach

Perspective 30°

A)

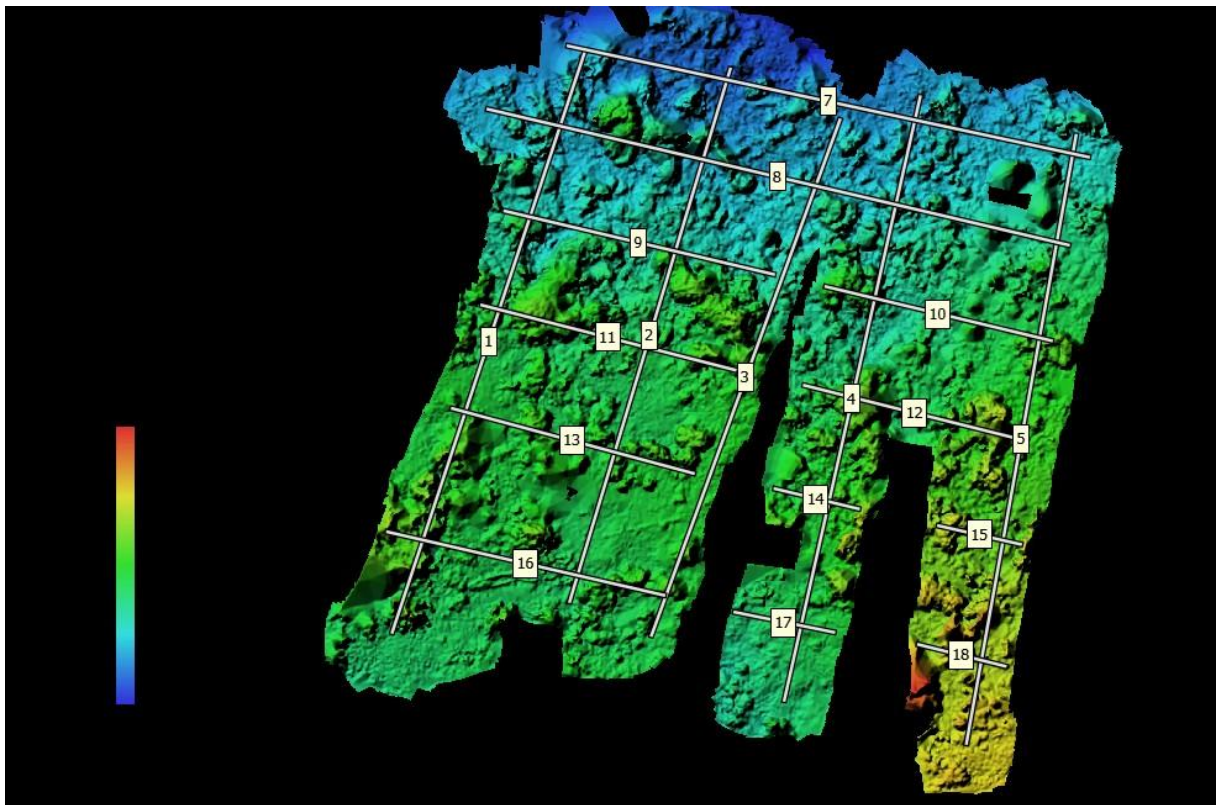


Figure 9: A) Metashape Agisoft generated 3-D model Bsc BEACH AND B) Metashape Agisoft generated DEM Bsc Beach, with the virtual chains used for the rugosity (Low → high is blue → red)

8.2.3 Jeff Davis

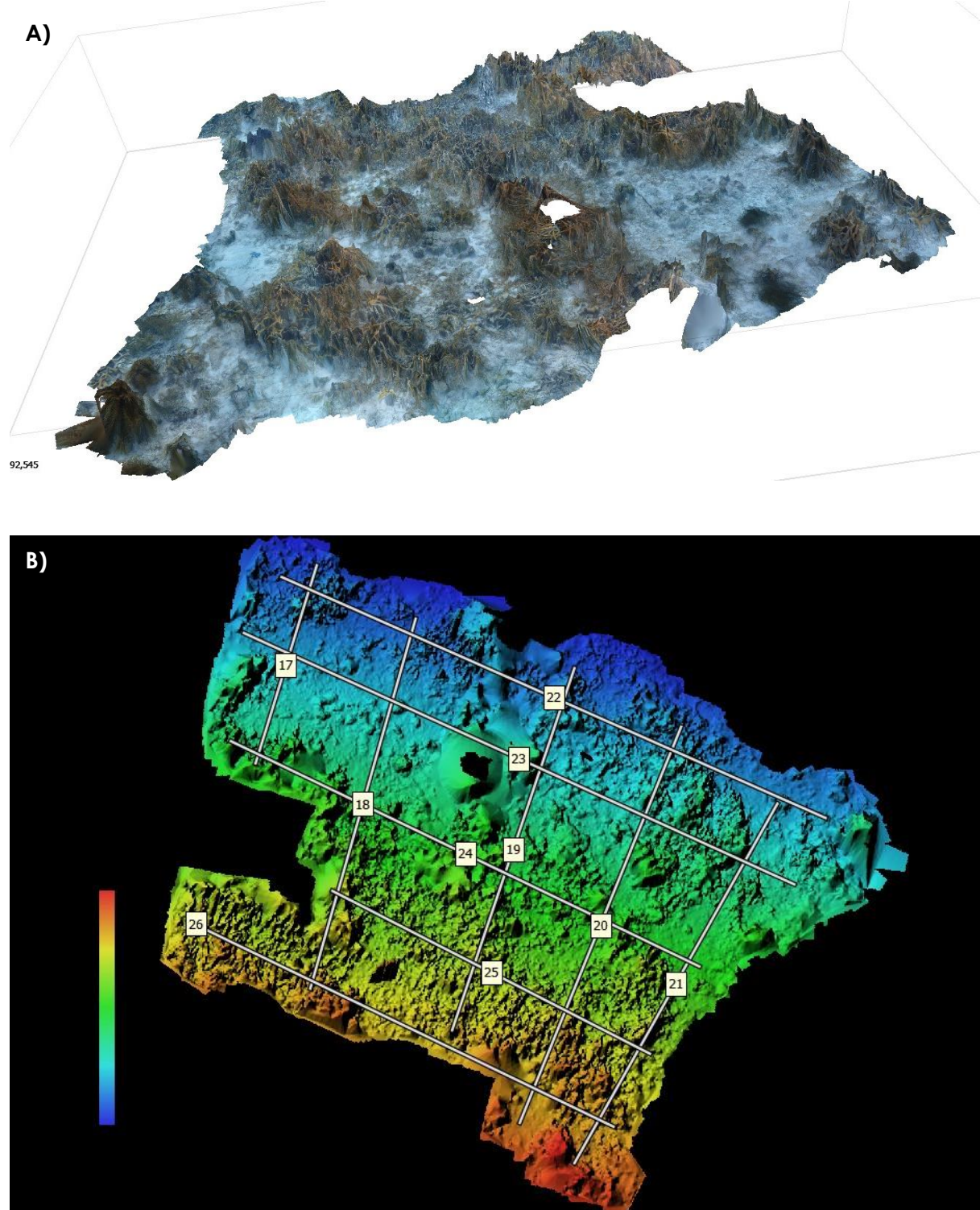
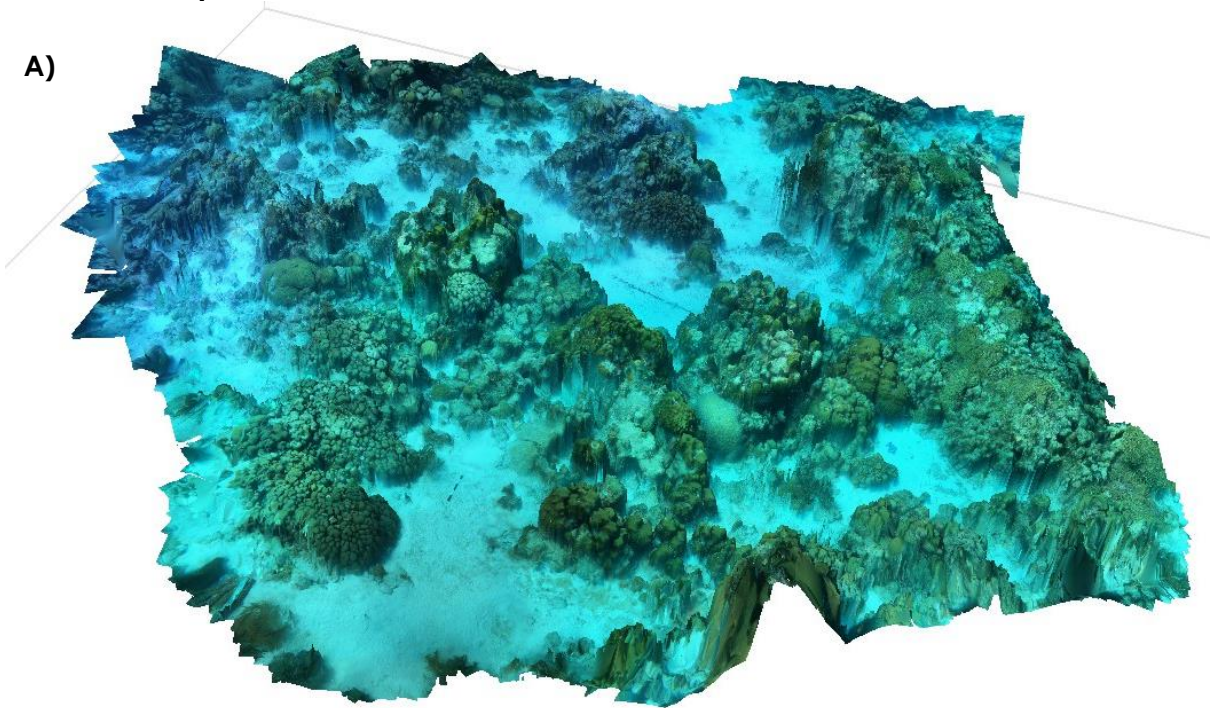


Figure 10: A) Metashape Agisoft generated 3-D model Jeff DAVIS AND B) Metashape Agisoft generated DEM Jeff Davis, with the virtual chains used for the rugosity (Low → high is blue → red)

8.2.4 1000 Steps

A)



vertices: 202,566

B)

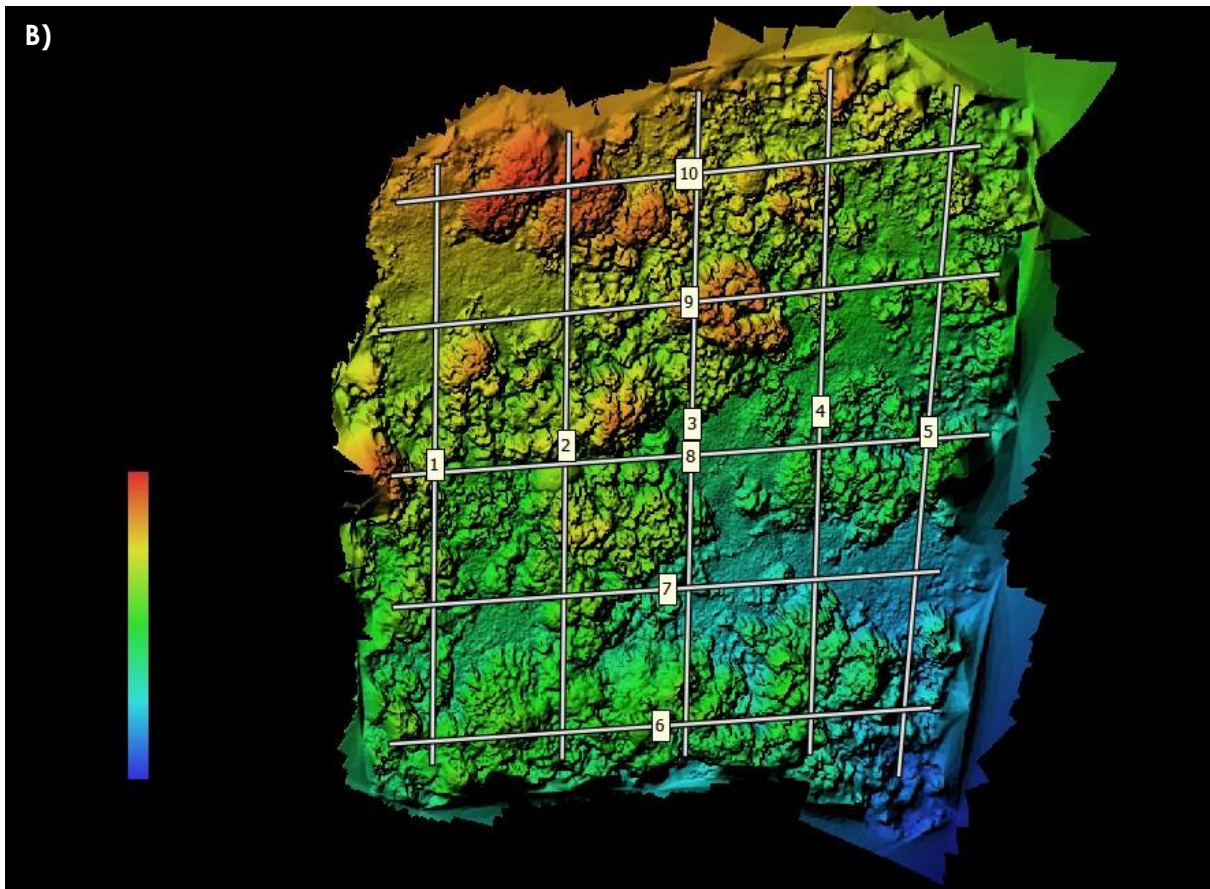


Figure 11: A) Metashape Agisoft generated 3-D model 1000 STEPS AND B) Metashape Agisoft generated DEM 1000 Steps, with the virtual chains used for the rugosity (Low → high is blue → red)

8.3 Moored ADCP results overview per locations

8.3.1 Park Tului

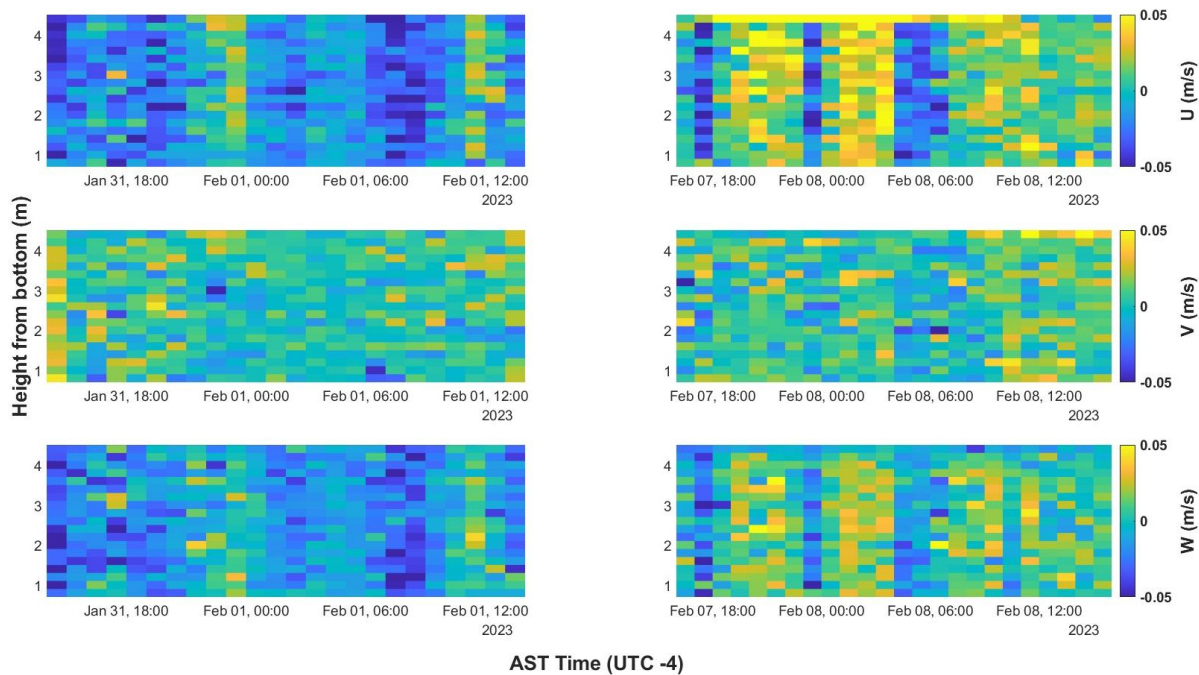


Figure 12: Hourly averaged longshore (U), cross-shore (V) and vertical (W) velocity over time for the first (left) and second (right) Park Tului measurements, with positive numbers in the northward, offshore and upward direction.

Figure 12 shows the measured velocity of the moored ADCP measurements at Park Tului at 31-01 and 07-02. Both measurements started in the afternoon, at 14:00 local time at 31-01 and 16:00 at 07-02. The ADCP was placed around 5m depth, close to the drop-off. In general, the flow velocity is low for both measurements, with velocities between the 0 and 0.05 m/s. From the measurements, no clear tidal signal can be discovered. For both measurements there are correlations visible between the longshore and vertical velocities. Any correlation between horizontal velocities and the vertical velocity could be partially explained by a large pitch or roll of the instrument. The pitch and roll were 0.75° and 2.5° for the 31-01 measurement and 0.1° and 1.3° for the 07-02 measurement. With the pitch and roll of the instrument being low for both measurements, this cannot fully explain the correlation in the velocities. Another important result is the difference in velocity in all directions between the 31-01 and the 07-02 measurement. The second measurement velocities in the opposite direction for most the measurement period. The measurements were taken in between the spring and neap tide, with the closest spring and neap tide at 28-01 (neap) and 05-02 (spring). This resulted in similar tidal amplitudes for both measurement days. Also, the measurement length ensures that for both measurements an entire tidal cycle is measured. However, a major difference in the measurements can be observed in the wind speed. The average wind speed for the measured days was 15.5 and 27 km/h on 31-01 and 07-02 respectively. With the wind coming from the east, as it does generally on Bonaire, a stronger wind can enhance the cross-shore velocities.

8.3.2 Bsc Beach

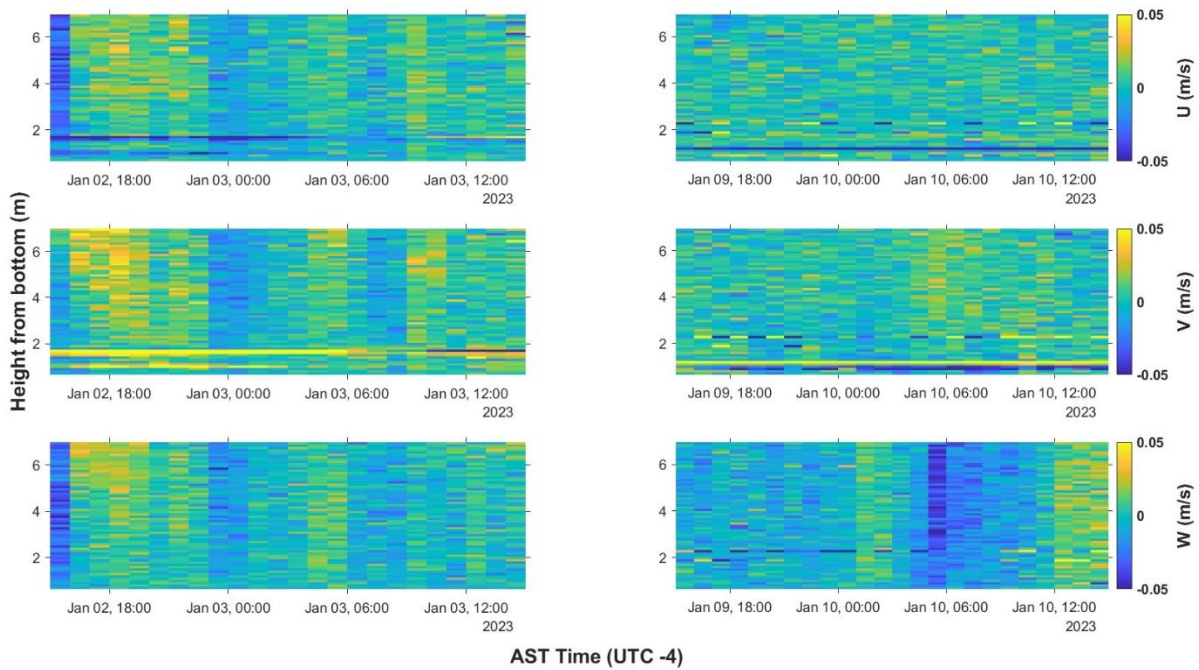


Figure 13: Hourly averaged longshore (U), cross-shore (V) and vertical (W) velocity over time for the first (left) and second (right) Bsc Beach measurements, with positive numbers in the northward, offshore and upward direction.

The moored ADCP measurements at Bsc Beach (Figure 13) were taken on 02-01 and 09-01. Both measurements were started at 15:15 and lasted for 25h. The ADCP was placed at 8m depth, close to the drop-off. In the data there is an irregularity visible between 1 and 2 meters from the bottom. These spikes in velocity may have been caused by something sitting in one of the ADCP beams and these data were not considered. Similar velocities were measured as at Park Tului, between 0 and 0.05 m/s. At Bsc Beach, however, the velocities were generally close to 0, with only on rare occasions a velocity increase up to 0.05 m/s. This occurred in the first measurement hours on 02-01 for the longshore velocity and around 5:00 AM on 09-01 for the vertical velocity. Unlike Park Tului, changes in velocity for a direction are not reflected in the velocities in the other direction. Even though the pitch and roll (3° and -8° , and -3° and -9° for 02-01 and 09-01 respectively) are much higher at Bsc Beach, the correlations between the velocities are not visible. The high longshore velocity in the first measurement hours on 02-01 are not likely explained by tidal movement, as the tidal amplitudes on 02-01 were much smaller than on 09-01, 10cm compared to 40cm. However, the higher tidal amplitudes on 09-01 are not reflected in tidal currents at all; there is barely any current during the measurement at 09-01. Also, there are no clear peaks in wind speed during the period of stronger currents on both days. There are, however, rain events on both the days during these periods. As rain events on Bonaire are often accompanied by surges in wind, it could be possible that strong wind occurred in those periods, but not long enough to show a large peak in the average wind speed.

8.3.3 Jeff Davis

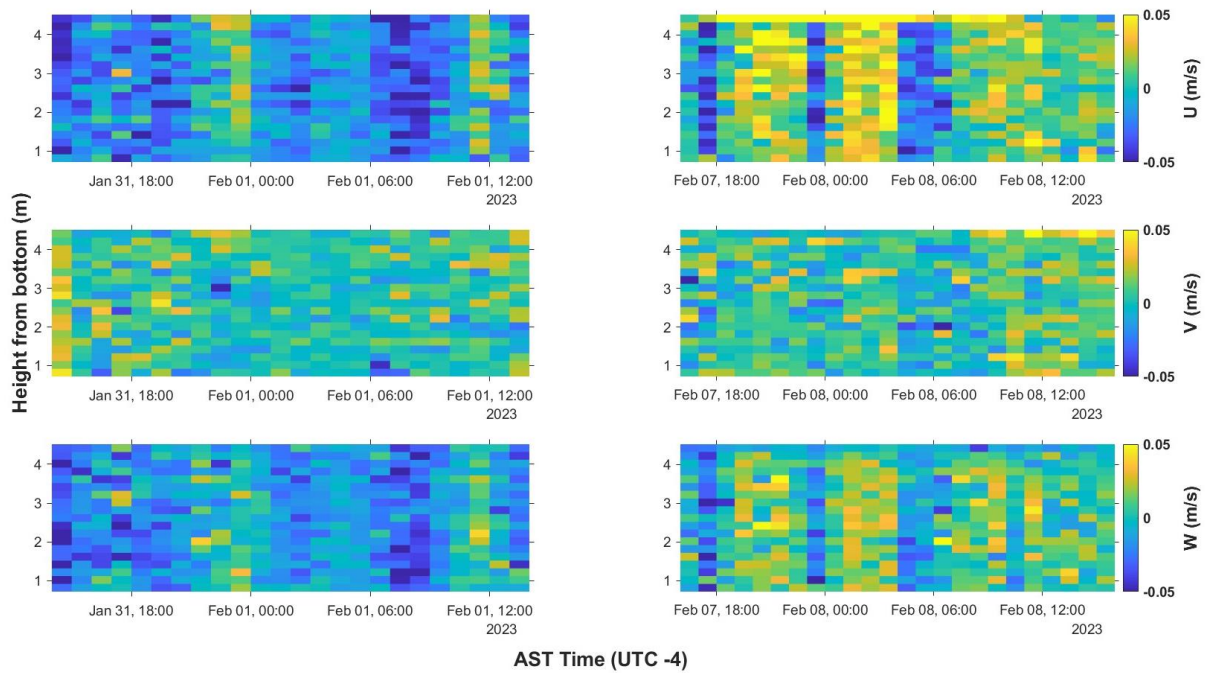


Figure 14: Hourly averaged longshore (U), cross-shore (V) and vertical (W) velocity over time for the first (left) and second (right) Jeff Davis measurements, with positive numbers in the northward, offshore and upward direction.

The data were collected at Jeff Davis was collected on 16-01 and 06-02 (Figure 14). The ADCP was placed at a depth of 4.5m again close to the drop-off. Both measurements started at 16:00 and lasted 26 and 27 hours. The first measurement was done with a vertical cell size of 10cm, the second with a cell size of 20cm. Higher velocities were measured during the second measurement. The increase in velocity between the measurements does not come from peaks in the velocity, but from a general increase in the velocity over the whole period. The tidal amplitudes for this period were around the 20cm on 16-01 and 35cm on 06-02. Although this does show a difference in tidal amplitude between the measurements, the periodicity of tides is not reflected in the hourly averaged velocity. There was, also, a major difference in wind speed between the two days, similar to Park Tului, with an average wind speed of 16.5 and 27.5 km/h for the two days. Again, it was a constant easterly wind. Where there were some patterns discernible in the velocities at Park Tului and Bsc Beach, the velocity distribution at Jeff Davis seems to be very random, there are no patterns of a logarithmic velocity profile or of fluctuations over time visible. It is important to note that this is an area where the drop-off occurs at a very shallow depth (~5m) and where the rugosity is high.

8.3.4 1000 Steps

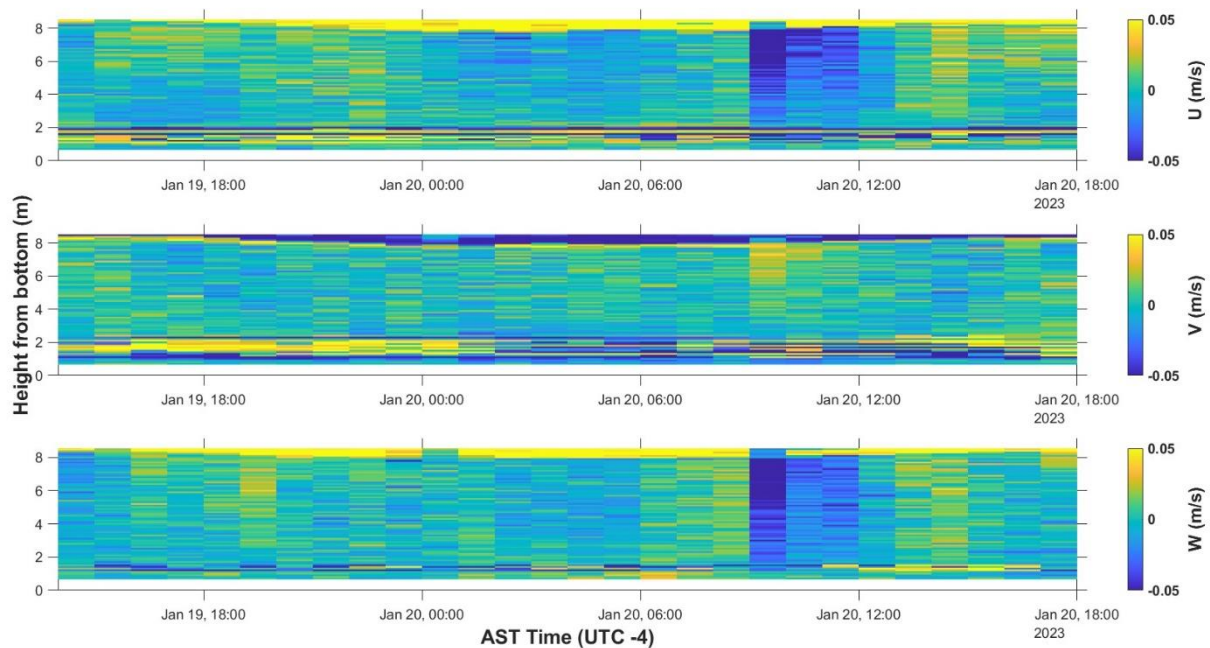


Figure 15: Hourly averaged longshore (U), cross-shore (V) and vertical (W) velocity over time for the 1000 Steps measurement, with positive numbers in the northward, offshore and upward direction.

1000 Steps is the only location that was measured only once (Figure 15). A second time was done, but due to an error, probably in the connection with the battery, no data were obtained. The measurement at 1000 Steps was done on 19-01 for 29 hours from 14:00. There are again irregularities between 1 and 2.5m from the bottom. This is probably again caused by interference in one of the beams. Contrary to Jeff Davis, higher velocities occurred here only for a brief period. The rest of the measurement time, the velocities were between the -0.05 and 0.05 m/s, like the other measurements. During the period of higher velocity, between hours 20 and 22, there is a clear negative peak in velocity in the longshore direction, accompanied by a negative peak in the vertical velocity. Again, the correlation between the horizontal velocities and the vertical velocity could be caused by a strong pitch and roll of the instrument. As the pitch and roll were -1.5° and 4° , it would not account for everything. The high peak in the currents do show a higher average wind speed than the rest of the period, but the around this time precipitation did again occur.